UNIMORE
UNIVERSITÀ DEGLI STUDI DI MODENA E REGGIO EMILIA

UNIVERSITÀ DEGLI STUDI DI MODENA E REGGIO EMILIA

Dottorato di ricerca in

Clinical and Experimental Medicine (CEM)
-
Medicina Clinica e Sperimentale

Ciclo XXXVIII

Refining Patient Risk Profiles in Hodgkin lymphoma Through Gene Expression Profiling and Spatial Transcriptomic Analysis

Candidato: Stefano Pozzi Matr. N. 184428

Relatore (Tutor): Prof. Stefano Luminari

Coordinatore del Corso di Dottorato: Prof. Marco Vinceti

Table of Contents

Abstract

Background

Classical Hodgkin lymphoma (cHL) is one of the most curable hematologic malignancies; however, a clinically relevant proportion of patients develops primary refractory disease or early relapse, conditions associated with inferior survival and limited salvage options. Early identification of high-risk patients remains a major unmet clinical need, particularly in the context of increasingly personalized therapeutic strategies. To address this issue, we investigated the biological determinants of disease aggressiveness by analyzing the reciprocal interactions between malignant Hodgkin and Reed–Sternberg (HRS) cells and the tumor microenvironment (TME), and evaluated their clinical impact on patient outcome.

Methods

We applied a morphology-driven, spatially resolved transcriptomic approach to characterize gene expression profiles of HRS cells ($CD30^+$) and the surrounding immune microenvironment ($CD45^+/CD30^-$) in lymph node biopsies from a matched cohort of cHL patients with divergent clinical courses, including relapsed/refractory (R/R^+) and relapse-free (R/R^-) cases. To assess the broader clinical relevance of these findings, digital barcoding–based bulk transcriptional profiling was performed in a retrospective monocentric training cohort (N = 155) comprising patients across all disease stages treated with standard first-line chemotherapy, and in an independent multicentric validation cohort. Gene expression data were correlated with progression-free survival (PFS) to derive and validate a biologically informed prognostic score.

Results

Spatial transcriptomic analyses revealed profound transcriptional differences within the HRS compartment, with aggressive R/R^+ cases displaying a marked loss of B-cell lineage identity and enhanced immunomodulatory signaling compared with R/R^- tumors. Importantly, we identified a clinically relevant protective role of non-malignant B cells within the TME. An inverse relationship between the abundance of HRS cells and normal B cells was consistently observed, suggesting that preservation of the non-tumoral B-cell compartment constrains tumor aggressiveness.

In the training cohort, expression of B-cell–related genes was significantly associated with improved PFS. This led to the development of a B-cell–specific gene-expression score capable

of stratifying patients according to risk of progression, independently of established clinical and radiomic factors. Notably, this score discriminated outcome even among patients with early-stage disease. The prognostic performance of the model was subsequently confirmed in the independent validation cohort.

Conclusions

Our findings define a biologically grounded and clinically meaningful prognostic framework in classical Hodgkin lymphoma. By bridging functional characterization of the tumor microenvironment with outcome-driven modeling, this study identifies preservation of the non-malignant B-cell compartment as an independent determinant of disease progression. B-cell–derived molecular signatures may therefore represent robust biomarkers to refine risk stratification and support more personalized clinical management of cHL patients.

Introduction

Overview of classical Hodgkin Lymphoma

Classical Hodgkin lymphoma (cHL) is well-defined subtype of B-cell lymphoma, accounting for approximately 10–15% of all lymphoma cases globally [1]. It is characterized by the presence of Hodgkin and Reed–Sternberg (HRS) cells embedded in a markedly inflammatory tumor microenvironment (TME). Despite its distinct biology, cHL is typically associated with high cure rates following first-line treatment. However, a subset of patients, approximately 5-10%, develop primary refractory disease, and another 10-20% relapsing after achieving an initial response. These cases often display more aggressive biological behavior and present significant clinical challenges, including lower response rates to salvage treatments and poorer long-term outcomes. The complex and dynamic TME in cHL plays a crucial role in tumor survival and immune evasion, suggesting that refractory disease is driven not only by intrinsic tumor characteristics but also by intricate interactions within the TME. These mechanisms may not be fully accounted for by traditional prognostic models, which largely depend on clinical and laboratory parameters. Recent advances in genomic and transcriptomic profiling have provided deeper insights into the molecular alterations and immune evasion mechanisms that contribute to treatment resistance, underscoring the potential for discovering novel biomarkers to enhance early risk stratification. Nevertheless, translating these findings into routine clinical practice remains challenging, necessitating further validation and integration with established prognostic tools. As the therapeutic landscape evolves with the introduction of immunotherapies and targeted agents, there is an urgent need to optimize patient care through risk-adapted treatment strategies. Early identification of patients at high risk for refractory or early-relapse disease would enable more intensive therapeutic interventions, while sparing low-risk individuals from overtreatment and reducing long-term toxicity. Integrating genomic insights with clinical and radiologic data provides a pathway toward precision medicine approaches that have the potential to transform the management of cHL, particularly for this challenging patient population.

Epidemiology

The overall global incidence of cHL is estimated at 0.98 cases per 100,000 individuals, with higher rates observed in Western countries [2,3], averaging 2–3 cases per 100,000 people. The disease shows a bimodal age distribution, with a peak incidence in young adults aged 20–30 years and a second peak in older adults, typically those aged 60 years and above [4,5]. cHL has a slight male predominance across all age groups, although the difference between males and females becomes more pronounced in older age groups [2,3]. Recent data from the Reggio Emilia Cancer Registry, covering the period from 1996 to 2020, offer further insights into the epidemiology of cHL in Northern Italy [6]. The age-standardized incidence rates (ASR) were 3.9 and 4.5 cases per 100,000 for males and females, respectively, with a male-to-female ratio of 1.3 based on absolute case numbers. The median age at diagnosis was 40 years, consistent with the disease's predilection for younger adults. Notably, 72.8% of cases occurred in individuals aged 18–65 years, 20.3% in those over 65 years, and 6.9% in patients younger than 18 years. Over the study period, cHL incidence remained relatively stable, ranging from 3.8 to 4.3 per 100,000. Encouragingly, the 5-year relative survival (RS) significantly improved, rising from 81.3% in the late 1990s to 92.4% during 2011–2015, reflecting advances in treatment and management. Mortality trends showed an initial increase until 2008, followed by a marked decline, with a mortality rate of 0.4 per 100,000 reported in 2020. Compared to the United States SEER data, incidence rates in Reggio Emilia are higher (4.2 vs. 2.4 per 100,000), whereas mortality is comparable (0.4 vs. 0.2 per 100,000) 2,6. These improvements in survival underscore the high curability of cHL, particularly with contemporary therapeutic protocols.

Histopathological classification of cHL

Classical Hodgkin lymphoma (cHL) is classified into four histological subtypes: nodular sclerosis (NSHL), mixed cellularity (MCHL), lymphocyte-rich (LRHL), and lymphocyte-depleted (LDHL) [7]. These subtypes differ in prevalence, pathological features, prognosis, and their association with Epstein–Barr virus (EBV). NSHL, the most common subtype, accounts for approximately 70% of cases and is characterized by fibrous nodules, often involving mediastinal lymph nodes. It primarily affects young adults and carries an excellent prognosis, with five-year survival rates exceeding 90% in early-stage disease [7,8]. MCHL represents 20–25% of cases, exhibits a heterogeneous cellular infiltrate, and is more frequently observed in older adults and immunocompromised patients, such as those with HIV. Its prognosis is

generally favorable but slightly inferior to NSHL, particularly in advanced stages [7,9]. LRHL accounts for roughly 5% of cases and is characterized by abundant small lymphocytes with sparse HRS cells, usually presenting at an early stage and associated with an excellent prognosis [7,10]. LDHL, the rarest subtype (<1%), shows a paucity of lymphocytes, numerous HRS cells, and extensive fibrosis or necrosis. It is more common in older adults and HIV-positive patients and is linked to poorer outcomes due to frequent advanced-stage disease and systemic symptoms [7,11]. Although subclassifying cHL into these histological subtypes is considered ideal in clinical practice, it has limited influence on treatment decisions. In cases where biopsy material is insufficient, precise subclassification may not be possible, and the diagnosis may simply be reported as cHL. This underscores that, despite their pathological and historical significance, the subtypes have minimal impact on modern therapeutic approaches.

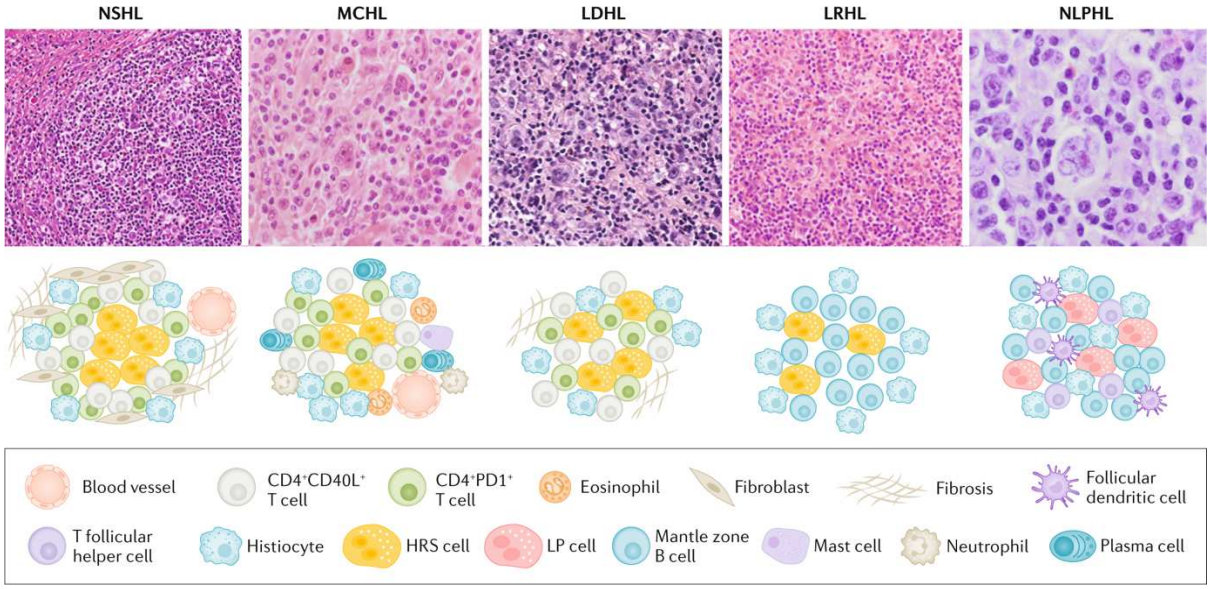

Figure 1. Morphological and cellular characteristics of Hodgkin Lymphoma [12]

Pathogenesis of cHL and the Role of the Tumor Microenvironment

Cellular Origin

Classical Hodgkin lymphoma (cHL) is defined by the presence of Hodgkin and Reed–Sternberg (HRS) cells, which are large, multinucleated B-cell–derived cells. Although these cells are sparse within the tumor, they are embedded in a distinctive tumor microenvironment (TME) rich in reactive immune cells, including T cells, eosinophils, macrophages, and plasma cells. The intricate interactions between HRS cells and the TME are central to cHL pathogenesis, promoting tumor survival, immune evasion, and disease progression. HRS cells originate from mature germinal center (GC) B cells, as demonstrated by clonally rearranged and somatically mutated immunoglobulin (Ig) genes [13]. In many cases, these immunoglobulin (Ig) genes carry deleterious mutations introduced by AID-driven somatic hypermutation, resulting in a non-functional B-cell receptor (BCR). Under normal physiological conditions, the lack of a functional BCR would trigger apoptosis in germinal center (GC) B cells. However, transformative events—including constitutive activation of survival pathways, AID-related somatic hypermutations, Epstein–Barr virus (EBV) infection, and microenvironmental signals—enable these pre-apoptotic cells to evade cell death, proliferate abnormally, and acquire a reprogrammed phenotype [14]. Although HRS cells are of B-cell origin, they show an almost complete loss of conventional B-cell markers, including CD20, CD19, CD22, and CD79, along with weak expression of PAX5, a critical B-cell transcription factor [15,16]. This loss of B-cell identity is further reinforced by promoter hypermethylation and epigenetic silencing of genes essential for B-cell differentiation [12]. Paradoxically, HRS cells aberrantly express markers typically associated with other hematopoietic lineages, including T-cell markers (CD2, CD3, CD4) and myeloid markers (CD15), further obscuring their B-cell origin [17]. Notably, HRS cells are consistently positive for CD30, a key molecule involved in their proliferation and survival, and express CD15 variably; both markers serve as important diagnostic markers [7].

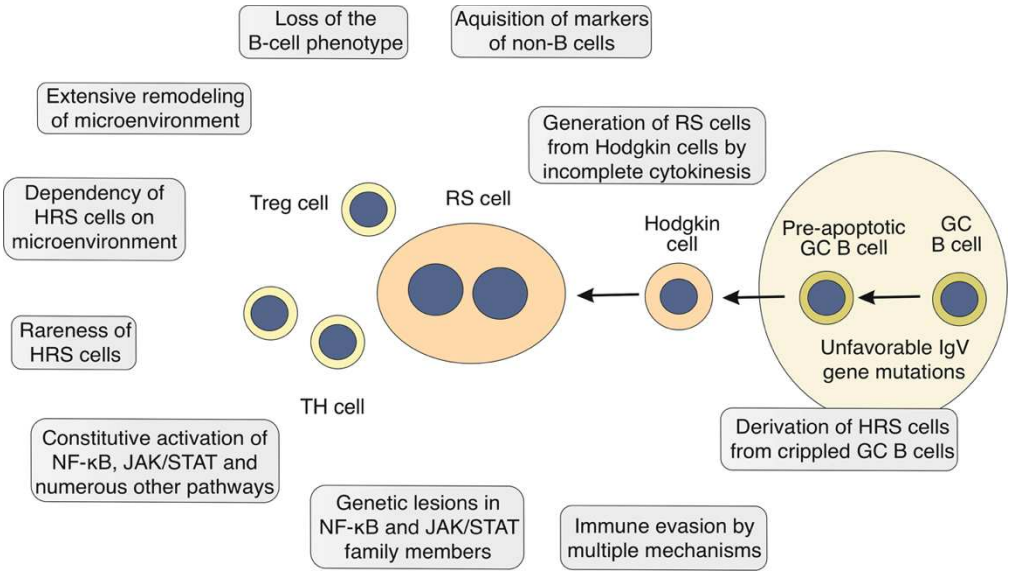

Figure 2. Hallmarks of HRS cells and cHL[18]

Key Pathways

The pathogenesis of cHL is driven by genetic and epigenetic alterations that activate key signaling pathways, notably NF-κB and JAK/STAT, which support HRS cell survival and proliferation. NF-κB activation can occur intrinsically through mutations in negative regulators such as NFKBIA and TNFAIP3, particularly in EBV-negative cases, or extrinsically via signals from the tumor microenvironment [12,19]. In EBV-positive cHL, which accounts for 30–40% of cases—especially in the MCHL and LDHL subtypes—the viral latent membrane protein 1 (LMP1) mimics CD40 signaling, further activating NF-κB and promoting HRS cell survival [20,21]. The JAK/STAT pathway is also commonly dysregulated, frequently involving mutations in SOCS1 and STAT6 [22]. These mutations lead to sustained hyperphosphorylation of STAT proteins, including STAT5A, STAT5B, and STAT6, resulting in the transcriptional activation of downstream oncogenic targets such as MYC, a master regulator of cell proliferation, growth, and apoptosis [23,24]. In parallel, members of the AP-1 transcription factor family (JUN, JUNB, BATF3) are constitutively expressed under the influence of NF-κB and JAK/STAT signaling, driving the expression of critical survival genes, including MYC and CD30 [24,25]. Constitutive activation of the PI3K/AKT pathway represents another central mechanism supporting HRS cell survival and proliferation [26]. This activation arises through multiple mechanisms, including loss-of-function mutations in ITPKB and/or GNA13, as well as signaling through TNFRSF family members (CD30, CD40, RANK) and G-protein–coupled receptors such as S1PR1 [27].

Moreover, HRS cells aberrantly express a broad array of receptor tyrosine kinases (RTKs), including PDGFRA, DDR1/2, EPHB1, TRKA, RON, CSF1R, and MET, which are activated by ligands present in the tumor microenvironment or through autocrine signaling loops [28,29]. The NOTCH1 pathway is also frequently active in HRS cells; ligand binding triggers receptor cleavage and nuclear translocation of the intracellular domain, leading to transcriptional programs that promote proliferation while further suppressing the B-cell differentiation program [30].

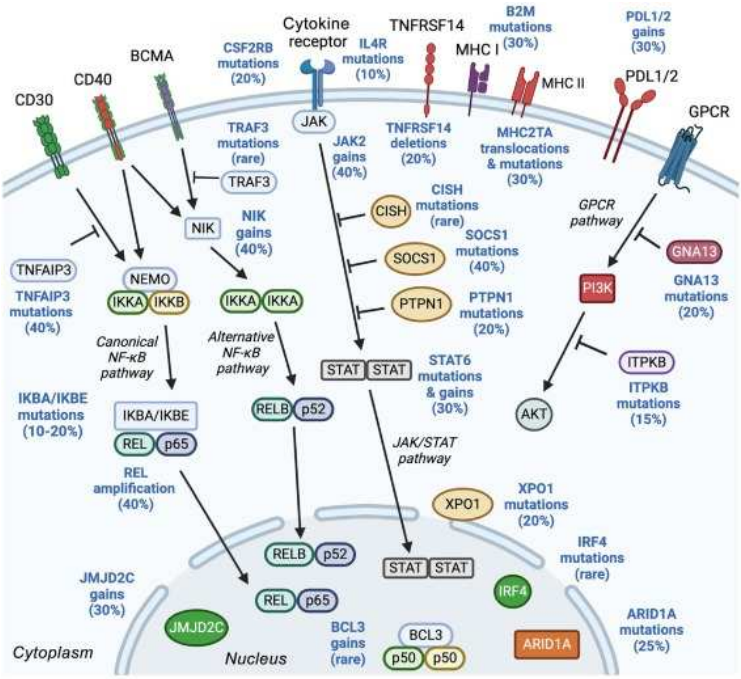

Figure 3. Main Signaling Pathways and Recurrent Genetic Lesions Involved in cHL [31]

Immune Evasion Mechanisms

Immune evasion represents a defining hallmark of classical Hodgkin lymphoma and is driven by recurrent genetic alterations that impair antigen presentation and suppress effective antitumor immune responses. A central mechanism involves the overexpression of the immune checkpoint ligands PD-L1 (CD274) and PD-L2 (PDCD1LG2), encoded within the chromosome 9p24.1 locus. Genetic alterations at this locus—including copy number gains, high-level amplifications, and chromosomal rearrangements—are present in the majority of cHL cases, with copy number gains being the most frequent event. The resulting overexpression of PD-L1 and PD-L2 leads to engagement of PD-1 receptors on cytotoxic T cells and natural killer (NK) cells, thereby inhibiting their effector functions and allowing HRS cells to evade immune

surveillance [32,33]. Additional mechanisms contributing to PD-L1/PD-L2 upregulation include Epstein–Barr virus (EBV) infection and transcriptional activation driven by 9p24.1 alterations, providing a strong biological rationale for PD-1 blockade, which has demonstrated remarkable clinical efficacy in cHL [34].

Beyond checkpoint activation, genetic disruption of antigen presentation pathways further facilitates immune escape. HRS cells frequently exhibit loss or downregulation of major histocompatibility complex (MHC) class I and II molecules, compromising recognition by $CD8^+$ cytotoxic T lymphocytes. This may result from translocations involving CIITA, the master regulator of MHC class II expression, or from inactivating mutations in B2M, an essential component of MHC class I [35,36]. Consequently, antigen-dependent T-cell–mediated cytotoxicity is markedly impaired. In addition, loss of CD58expression due to mutations or deletions disrupts NK cell–mediated recognition and killing of HRS cells. Collectively, PD-L1/PD-L2 overexpression, defective antigen presentation, and loss of NK cell co-stimulatory signals cooperate to establish a profoundly immunosuppressive tumor microenvironment that enables HRS cell persistence and disease progression [37].

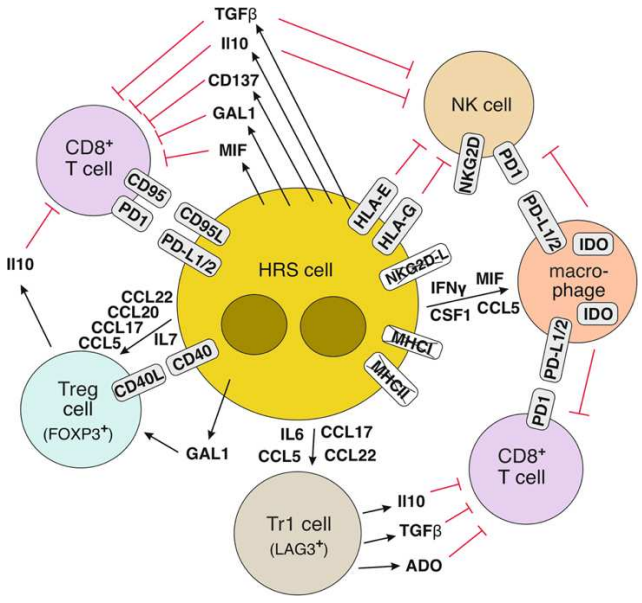

Figure 4. Immune evasion mechanisms in cHL[18]

The Tumor Microenvironment

TME, which surrounds the rare HRS cells that constitute approximately 1% of the total tumor mass, represents a highly complex and dynamic ecosystem of immune and stromal elements that are actively reprogrammed to support tumor growth and survival. HRS cells secrete a broad array of immunomodulatory cytokines, including IL-10 and TGF-β, as well as chemokines such as CCL5, CCL17, and CCL22, which promote the recruitment of regulatory T cells (Tregs), Th2-polarized $CD4^+$ T cells, and macrophages, thereby suppressing effective antitumor immune responses [19]. This extensive cellular and molecular reprogramming establishes a profoundly immunosuppressive milieu that shields HRS cells from immune-mediated elimination and facilitates their persistence.

The cellular composition of the TME differs markedly among the histological subtypes of cHL, reflecting both biological heterogeneity and subtype-specific pathogenic mechanisms. Nodular sclerosis Hodgkin lymphoma (NSHL) is distinguished by prominent fibrosis and extensive fibroblast involvement, whereas mixed cellularity HL (MCHL) displays a polymorphous inflammatory infiltrate rich in eosinophils, neutrophils, and macrophages. In contrast, lymphocyte-depleted HL (LDHL) is characterized by an abundance of HRS cells and macrophages with a relative paucity of lymphocytes, while lymphocyte-rich HL (LRHL) exhibits a predominance of non-malignant lymphocytes and B cells [38]. These distinct microenvironmental patterns underscore the critical and subtype-dependent role of the TME in shaping disease behavior and progression. Notably, macrophages—particularly tumor-associated macrophages (TAMs)—emerge as key mediators of immune evasion and tumor progression in cHL. Steidl et Al. have demonstrated that a high density of $CD68^+$ TAMs is associated with inferior overall survival (OS) and progression-free survival (PFS) [39]. TAMs actively suppress cytotoxic T-cell responses while promoting HRS cell survival, establishing their role as both adverse prognostic biomarkers and attractive therapeutic targets [40]. Moreover, TAMs express PD-L1, further reinforcing the immunosuppressive tumor microenvironment through engagement of PD-1 on T cells. In addition to macrophages, eosinophils and mast cells contribute to HRS cell proliferation by providing ligands such as CD30L, which activates the CD30 receptor on HRS cells [41].

Recent transcriptomic and single-cell RNA sequencing analyses have further refined our understanding of the cHL microenvironment, revealing distinct immunosuppressive cell populations, including $LAG3^+$ T cells, as well as macrophage-associated markers such as CSF1R, both of which correlate with disease aggressiveness and clinical outcome [42,43]. LAG3

(lymphocyte activation gene 3) is an inhibitory immune checkpoint receptor structurally related to CD4 that binds MHC class II molecules and attenuates T-cell activation, thereby contributing to immune dysfunction within the TME [44].

$CD4^+$ T cells represent the most abundant immune population in cHL and are frequently observed in close physical proximity to HRS cells, forming characteristic "rosettes." These interactions are mediated by multiple receptor–ligand pairs, including CD40–CD40L and CD80/CD86–CD28, as well as adhesion molecules such as CD11a/CD18 on T cells and CD54 on HRS cells. Together with cytokine-mediated signaling, including IL-3 secretion, these direct cellular interactions are critical for sustaining HRS cell survival [45]. Additional non-malignant components of the TME, such as fibroblasts and dendritic cells, further contribute to tumor support by secreting pro-survival factors including IL-7, IL-15, and hepatocyte growth factor (HGF) [46,47].

Collectively, the survival and proliferation of HRS cells are critically dependent on sustained interactions with a highly specialized and immunosuppressive tumor microenvironment. Therapeutic strategies aimed at disrupting these pro-tumorigenic cellular and molecular interactions hold significant promise for restoring antitumor immunity and improving clinical outcomes in patients with cHL.

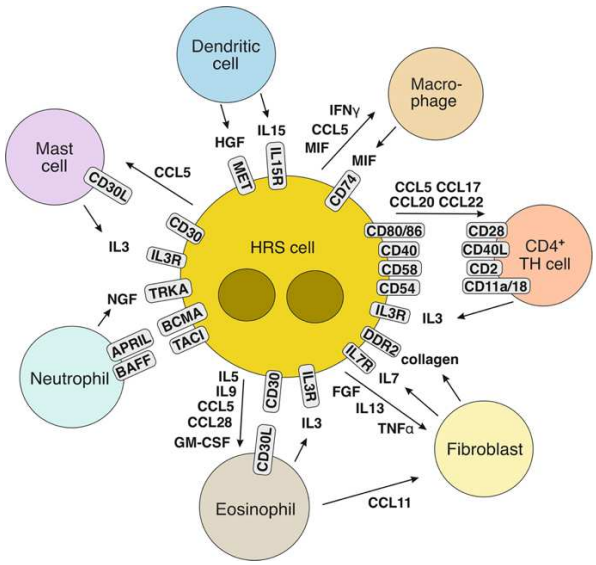

Figure 5. Microenvironmental Interactions in cHL Supporting HRS-cell Survival and Proliferation [18]

Staging and Risk Prognostication

The Ann Arbor staging system, updated by the 2014 Lugano classification, remains the standard framework for staging classical Hodgkin lymphoma. This system categorizes disease into stages I through IV according to the number of involved lymph node regions, their distribution relative to the diaphragm, and the presence of systemic "B symptoms," including fever, night sweats, and unexplained weight loss. The presence of bulky disease—defined as a mediastinal mass exceeding one-third of the thoracic diameter or a nodal mass greater than 10 cm—represents an additional prognostic factor with important implications for treatment planning [48].

Risk stratification incorporates Ann Arbor staging alongside other clinical variables. For patients with early-stage disease, risk assessment is most commonly based on the prognostic models developed by the European Organisation for Research and Treatment of Cancer (EORTC) and the German Hodgkin Study Group (GHSG). These models classify patients as having favorable or unfavorable risk profiles according to a combination of clinical and laboratory factors, including bulky disease, age ≥50 years, elevated erythrocyte sedimentation rate (ESR >50 mm/h, or >30 mm/h in the presence of B symptoms), and involvement of three or more lymph node regions [49]. Such stratification frameworks are essential for guiding risk-adapted treatment strategies aimed at optimizing disease control while minimizing unnecessary treatment-related toxicity.

In advanced-stage classical Hodgkin lymphoma, the International Prognostic Score (IPS) remains one of the most widely used risk stratification tools and is also commonly applied to patients with stage IIB disease presenting with unfavorable features, such as B symptoms or bulky mediastinal involvement. The IPS was originally derived from a cohort of more than 5,000 patients treated predominantly with ABVD (doxorubicin, bleomycin, vinblastine, and dacarbazine) or MOPP (mechlorethamine, vincristine, procarbazine, and prednisone) regimens and incorporates seven clinical parameters: age ≥45 years, male sex, stage IV disease, anemia (hemoglobin <10.5 g/dL), lymphopenia (<600/μL), leukocytosis (≥15,000/μL), and hypoalbuminemia (<4 g/dL). This score predicts five-year progression-free survival (PFS) and overall survival (OS), with increasing scores reflecting a higher risk of relapse [50].

A subsequent validation study published in 2012 evaluated the performance of the IPS in the context of contemporary treatment approaches in a cohort of 740 patients. This analysis expanded the applicability of the IPS to include patients with early-stage disease and unfavorable characteristics, such as B symptoms or bulky mediastinal masses (≥10 cm), as well

as individuals older than 65 years. The study confirmed the continued prognostic relevance of the IPS in the modern therapeutic era, reporting five-year PFS and OS rates ranging from 62% to 88% and from 67% to 98%, respectively, according to IPS category [51].

Recent advances have led to the development of the Advanced-Stage Hodgkin Lymphoma International Prognostic Index (A-HIPI), a next-generation risk stratification model designed to refine prognostic assessment in classical Hodgkin lymphoma. Developed by the Hodgkin Lymphoma International Study for Individual Care (HoLISTIC) Consortium, the A-HIPI leverages contemporary patient cohorts, modern treatment outcomes, and advanced statistical modeling to provide a more granular and individualized risk evaluation. The A-HIPI was derived from a large pooled analysis of clinical data from more than 4,000 patients with newly diagnosed advanced-stage Hodgkin lymphoma (stage IIB, III, and IV) enrolled in eight international phase III clinical trials. The model incorporates six prognostic variables—age, disease stage, bulky disease, hemoglobin level, absolute lymphocyte count, and serum albumin—each weighted according to its independent association with clinical outcomes in the derivation cohort. These weighted variables generate a cumulative risk score that stratifies patients into distinct prognostic groups. External validation was performed in over 1,400 contemporaneously treated patients drawn from four real-world cHL registries. Across validation cohorts, the A-HIPI demonstrated superior predictive performance for both 5-year overall survival (OS) and progression-free survival (PFS) in adults aged 18–65 years when compared with the traditional International Prognostic Score (IPS). Importantly, robust model calibration supports its applicability across diverse patient populations, underscoring its clinical utility for guiding risk-adapted treatment decisions in advanced-stage Hodgkin lymphoma [52,53].

For clinical implementation, the A-HIPI score can be calculated using the online tool provided by the HoLISTIC Consortium (https://holistic- calculator.web.app/). While established prognostic models such as the IPS and the newer A-HIPI have improved risk assessment in advanced-stage cHL, their dependence on clinical and laboratory parameters highlights the need for more biologically informed approaches. As therapeutic strategies continue to evolve, incorporating advanced imaging modalities, molecular biomarkers, and other dynamic patient-specific parameters promises to enhance the accuracy and granularity of risk stratification. This shift toward personalized, biology-driven prognostication has the potential to guide more precise, risk-adapted therapies and ultimately improve clinical outcomes for patients with cHL.

Risk-Adapted and Response-Adapted Initial Therapy

Initial treatment of classical Hodgkin lymphoma (cHL) is guided by both baseline risk stratification and early assessment of treatment response. Risk-adapted strategies consider factors such as disease stage, tumor bulk, and established prognostic indicators to determine the intensity of initial therapy. In early-stage disease, the standard of care traditionally involves combined modality therapy, consisting of short courses of systemic chemotherapy with ABVD (doxorubicin, bleomycin, vinblastine, dacarbazine) followed by involved-field radiation therapy (IFRT). Patients with advanced-stage disease, in contrast, generally receive longer courses of chemotherapy, often without routine radiation. More recently, response-adapted approaches have introduced a dynamic element to this risk-based framework, allowing treatment intensity to be modified based on early indicators of tumor response. Functional imaging with fluorodeoxyglucose positron emission tomography (FDG-PET) scans are crucial in guiding therapy adjustments.

The implementation of a standardized 5-point scale for PET interpretation has improved both the reproducibility and predictive value of FDG-PET imaging, enabling the detection of residual lymphoma that may be missed on conventional CT scans [54]. Interim PET scans, typically performed after two cycles of therapy, can identify patients who achieve an early metabolic response. For these patients, therapy can often be de-escalated, potentially reducing or omitting radiation and thereby minimizing long-term treatment-related toxicity. Conversely, patients with persistently positive interim PET scans may benefit from treatment intensification, such as escalation to BEACOPP (bleomycin, etoposide, doxorubicin, cyclophosphamide, vincristine, procarbazine, prednisone) or prolongation of chemotherapy duration.

Multiple studies have shown that a positive FDG-PET scan at the end of therapy is associated with a markedly increased risk of disease recurrence and serves as a stronger predictor of progression-free survival (PFS) and overall survival (OS) than conventional prognostic factors [55,56]. Recent clinical trials incorporating novel agents, such as brentuximab vedotin or immune checkpoint inhibitors, have primarily relied on end-of-treatment PET results rather than interim scans. Consequently, the role of interim PET in guiding therapy adaptation in the context of these newer treatments remains uncertain [57,58]. While PET-adapted strategies are well established for conventional chemotherapy regimens, further investigation is needed to determine whether early metabolic responses reliably inform treatment decisions when novel agents are integrated into first-line therapy, or if alternative approaches are required.

Early-Stage Favorable HL

Current practice for early-stage favorable-prognosis Hodgkin lymphoma involves short-course chemotherapy in combination with involved-field radiation therapy (IFRT) directed solely at the affected lymph node regions. A pivotal study demonstrated no significant differences in treatment response, progression-free survival (PFS), or overall survival (OS) among patients receiving varying cycles of ABVD chemotherapy and IFRT doses. These findings established two cycles of ABVD followed by 20 Gy IFRT as the standard regimen for patients with early-stage favorable-risk disease [59].

Early-Stage Unfavorable HL

The optimal chemotherapy regimen, number of cycles, radiation dose, and field size in early-stage Hodgkin lymphoma remain areas of active investigation. The standard approach for early-stage unfavorable-risk disease typically consists of four cycles of ABVD followed by involved-site radiation therapy (ISRT) at 30 Gy [60]. However, the role of radiotherapy in patients achieving a complete metabolic response on interim PET continues to be debated. Key trials, including the UK National Cancer Research Institute RAPID study and the EORTC/LYSA/FIL H10 study, have shown that omitting radiotherapy may compromise disease control, even in patients with negative interim PET scans.

Management of patients with PET2-positive disease is particularly challenging. The H10 trial supports early treatment intensification with escalated BEACOPP in PET2-positive cases, whereas the RAPID study indicates that the prognostic impact depends on the Deauville score, with intensification typically reserved for patients scoring 5. For those with a Deauville score of 4, an alternative strategy often involves additional chemotherapy cycles followed by ISRT, with ongoing reassessment of treatment response [61,62,63]. Subsequent studies have explored intensified chemotherapy approaches, such as combinations of escalated BEACOPP and ABVD, which improved freedom from treatment failure but did not translate into an overall survival benefit [64]. Moreover, recent trials incorporating novel agents, including brentuximab vedotin and PD-1 inhibitors, have demonstrated favorable safety profiles and excellent disease control, with ongoing studies comparing these regimens to standard treatment approaches [65,66].

Advanced-Stage Disease

In patients with advanced-stage Hodgkin lymphoma (stages IIB–IV), treatment goals focus on achieving durable remissions while minimizing long-term toxicity. The choice of chemotherapy intensity remains a topic of debate: less intensive regimens such as ABVD are associated with lower toxicity but higher relapse rates, whereas more intensive approaches like escalated BEACOPP offer superior progression-free survival (PFS) at the cost of increased treatment-related toxicity [67,68].

PET-based response assessment has become central to guiding individualized therapy intensity. Early metabolic responses allow for treatment de-escalation, while suboptimal responses prompt intensification. The RATHL study demonstrated that PET-guided modifications maintain treatment efficacy while potentially reducing toxicity: patients with negative PET scans after two cycles of ABVD safely omitted bleomycin without compromising long-term outcomes, whereas PET-positive patients were escalated to BEACOPP without an increased risk of secondary malignancies [69].

Attempts to incorporate high-dose chemotherapy (HDCT) and autologous stem cell transplantation (ASCT) into frontline therapy for poor-risk patients have not yielded additional survival benefits [70]. However, the integration of novel agents has markedly improved outcomes. Brentuximab vedotin (BV), combined with standard chemotherapy, significantly enhanced first-line outcomes in advanced-stage disease [57]. The ECHELON-1 trial demonstrated superior PFS and overall survival (OS) for BV-AVD compared with ABVD, establishing it as a preferred first-line regimen. Building on this, the German Hodgkin Study Group (GHSG) incorporated BV into BEACOPP-based therapy; the BrECADD regimen (brentuximab vedotin, etoposide, cyclophosphamide, doxorubicin, dacarbazine, dexamethasone) proved well-tolerated and more effective than escalated BEACOPP, improving 4-year PFS in the randomized HD21 trial [71].

Immune checkpoint inhibitors, particularly anti–PD-1 antibodies, have further enhanced frontline outcomes [58,72]. The S1826 trial, comparing BV-AVD to nivolumab plus AVD (N-AVD), reported superior PFS in the N-AVD arm, with subgroup analyses highlighting particularly favorable outcomes in patients over [60]. These findings underscore the promise of N-AVD as a first-line option for older adults, a population in which treatment decisions are often limited by reduced tolerance to intensive chemotherapy regimens [73].

In summary, the management of classical Hodgkin lymphoma has increasingly shifted toward a personalized, risk-adapted approach. Interim PET-guided strategies and the incorporation of

novel agents have improved progression-free and overall survival while minimizing treatment-related toxicity. Regimens such as nivolumab plus AVD (N-AVD) and BrECADD allow therapy intensity to be tailored according to patient risk, and ongoing research continues to refine these strategies. Despite being among the most curable malignancies, with early-stage disease achieving cure rates exceeding 90%, cHL remains a clinical challenge in advanced-stage or refractory cases. Five-year survival approximates 90% for localized disease but decreases to around 80% for advanced stages. Moreover, long-term survivors may experience late complications related to therapy, underscoring the importance of optimizing both frontline treatment and survivorship care.

Management of Relapsed and Refractory Classical Hodgkin Lymphoma

Challenge of Refractory and Relapsing Disease

Relapsed and refractory (R/R) classical Hodgkin lymphoma (cHL) remains a major clinical challenge. Approximately 5–10% of patients exhibit primary refractory disease, while an additional 10–20% experience relapse after initially achieving a response [74]. Primary refractory disease is defined as the failure to attain a complete or partial response to first-line therapy, or progression of disease within three months of completing treatment [1,74,75]. These patients generally have a poorer prognosis compared to those with late relapse, exhibiting lower response rates to salvage chemotherapy and inferior survival outcomes.

Current Standard of Care

The treatment of relapsed or refractory (R/R) classical Hodgkin lymphoma (cHL) has traditionally centered on salvage chemotherapy followed by high-dose chemotherapy (HDCT) and autologous stem cell transplantation (ASCT), which provides durable responses in approximately 50% of patients. Randomized trials have demonstrated the superiority of this approach in terms of progression-free survival (PFS) and overall survival (OS) compared with chemotherapy alone [76]. Common salvage regimens include ICE (ifosfamide, carboplatin, etoposide) and DHAP (dexamethasone, cytarabine, cisplatin), as well as combination protocols such as BEGEV (bendamustine, gemcitabine, vinorelbine) and IGEV (ifosfamide, gemcitabine, vinorelbine). These regimens achieve partial or complete responses in roughly 50–70% of

patients, enabling many to proceed to ASCT. However, no randomized studies have directly compared the efficacy of these salvage regimens, leaving the optimal approach uncertain [77].

While ASCT can provide durable remission, certain factors—including primary refractory disease, bulky relapse, and persistent PET positivity after salvage therapy—substantially reduce the likelihood of success. The decision to proceed to transplant in patients achieving only a partial response to second-line therapy remains debated; nevertheless, achieving a negative PET prior to ASCT has emerged as one of the strongest predictors of post-transplant outcomes [78,79,80]. Patients with primary refractory disease generally exhibit lower response rates to salvage chemotherapy than those with late relapse, limiting their eligibility for ASCT and reducing the probability of sustained remission [81]. Consequently, primary refractoriness represents a major adverse prognostic factor prior to salvage therapy, strongly impacting both survival and treatment outcomes.

Novel Agents and Emerging Strategies

Recent advances have introduced novel agents, including brentuximab vedotin (BV) and immune checkpoint inhibitors (CPIs), which have transformed the management of relapsed or refractory (R/R) classical Hodgkin lymphoma. These therapies provide valuable options for patients who are chemoresistant, frail, or ineligible for autologous stem cell transplantation (ASCT).

Brentuximab vedotin is an anti-CD30 antibody-drug conjugate that selectively delivers monomethyl auristatin E, leading to cell cycle arrest and apoptotic death of CD30-positive tumor cells. Initially approved for R/R cHL based on a pivotal phase II trial demonstrating an overall response rate (ORR) of 75% and a complete response (CR) rate of 34% as monotherapy, BV has become a cornerstone of R/R cHL treatment [82]. When combined with salvage chemotherapy, BV further increases CR rates compared to monotherapy, enabling a greater proportion of patients to proceed to ASCT [83,84]. AETHERA trial demonstrated that BV consolidation post-ASCT significantly improved PFS in high-risk patients, particularly those with primary refractory disease [85].

Immune checkpoint inhibitors (CPIs), particularly PD-1 inhibitors such as nivolumab and pembrolizumab, have emerged as highly effective salvage therapies in relapsed or refractory (R/R) classical Hodgkin lymphoma, especially for patients who are ineligible for autologous stem cell transplantation (ASCT) or have received multiple prior therapies. In the KEYNOTE-087 trial, pembrolizumab demonstrated high overall response rates (ORRs) across various patient subgroups, including those with primary refractory disease, supporting its approval for R/R cHL [86,87].

Historically, chemorefractory patients were considered poor candidates for ASCT; however, recent studies indicate that anti–PD-1 therapy prior to transplantation can induce significant responses and improve survival outcomes even in primary refractory cases. Evidence suggests that CPIs may exert a chemosensitizing effect, enhancing the efficacy of subsequent salvage chemotherapy [88,89,90]. Interestingly, one study reported that achieving a complete metabolic response before ASCT was not a significant predictor of post-transplant progression-free survival (PFS), implying that even a partial response following CPI therapy may suffice to proceed to transplantation, thereby expanding ASCT eligibility for chemorefractory patients [89].

A pivotal randomized trial comparing pembrolizumab with brentuximab vedotin in R/R cHL demonstrated superior PFS with pembrolizumab, establishing PD-1 blockade as the preferred

option for patients relapsing after ASCT or ineligible for transplant [91]. Furthermore, combination strategies such as BV plus nivolumab have shown promising results, achieving high rates of complete metabolic response with lower toxicity than traditional salvage regimens [92]. These approaches are particularly advantageous for patients who are chemoresistant or frail and unable to tolerate intensive chemotherapy.

Challenges and Future Directions

Despite recent advancements, managing R/R cHL remains challenging due to the heterogeneity of treatment responses. Current prognostic models, such as the IPS and A-HIPI rely on baseline clinical and laboratory parameters but fail to capture the underlying biological diversity of cHL. This limitation makes it difficult to accurately identify high-risk patients, potentially leading to either undertreatment or overtreatment. Additionally, these models do not incorporate dynamic response markers like interim PET scans, which are crucial for refining prognosis based on treatment response. To overcome these limitations, integrating advanced molecular profiling, including transcriptomic analysis, with radiomic approaches offers promising solutions. Combining gene expression data with quantitative imaging features can provide a more comprehensive risk stratification, enabling personalized therapies that maximize efficacy while minimizing toxicity.

Emerging Technologies and Molecular Biomarkers

To overcome the limitations of current prognostic models, novel technologies and molecular biomarkers are increasingly being investigated to refine risk stratification and enable more personalized treatment approaches.

Radiomics

Radiomics, an advanced approach to imaging analysis, has emerged as a promising strategy to improve prognostication and risk stratification in Hodgkin lymphoma. By extracting high-dimensional quantitative features from imaging modalities such as FDG-PET, radiomics provides detailed information on tumor biology that extends beyond conventional visual assessment. When integrated with clinical and molecular data, these features can refine risk stratification and support more informed treatment decisions. Among PET-derived metrics, the

maximum standardized uptake value (SUVmax) is widely used to identify and characterize lesions and serves as a reliable indicator of tumor metabolic activity, aggressiveness, and response to therapy [93]. However, SUVmax captures only the single most metabolically active voxel and fails to account for spatial heterogeneity of tracer uptake within the tumor, a key feature of lymphoma biology referred to as intratumoral heterogeneity [94]. In Hodgkin lymphoma, several radiomic and metabolic parameters that better reflect disease burden and spatial complexity have shown increasing prognostic relevance, including metabolic tumor volume (MTV), total lesion glycolysis (TLG), and maximum tumor dissemination (Dmax). MTV quantifies the volume of tumor tissue exhibiting FDG uptake above a predefined threshold, thereby providing an estimate of the total metabolically active tumor burden. Consistently across multiple studies, elevated MTV has been associated with inferior progression-free and overall survival in patients with Hodgkin lymphoma [95,96,97].

Total lesion glycolysis (TLG) integrates volumetric and metabolic information by combining metabolic tumor volume (MTV) with the intensity of FDG uptake, and is calculated as the product of MTV and the mean SUV of all lesions. By capturing both tumor burden and overall metabolic activity, TLG provides a more comprehensive assessment of disease aggressiveness. Elevated TLG values, reflecting extensive and highly metabolically active disease, have been shown to be strong predictors of adverse treatment outcomes [98,99]. Despite their prognostic relevance, the routine clinical application of MTV and TLG remains limited by the lack of standardized acquisition and segmentation methodologies.

Maximum tumor dissemination (Dmax) is a more recently proposed PET-derived metric, defined as the greatest distance between the two most distant hypermetabolic lesions. Increasing evidence indicates that higher Dmax values are associated with biologically aggressive disease and inferior clinical outcomes [100,101,102]. Importantly, the integration of radiomic parameters with clinical and molecular data is gaining momentum as a means to enhance prognostic accuracy in classical Hodgkin lymphoma.

A notable radiogenomic study underscored the independent prognostic significance of Dmax, demonstrating its association with reduced progression-free survival in patients treated with ABVD who nonetheless achieved a complete metabolic response on interim PET. High Dmax was linked to an immunosuppressive tumor microenvironment, characterized by decreased naïve B cells and $CD8^+$ T cells and increased PD-L1 expression. In contrast, tumors with low Dmax showed enrichment of immune-related markers such as CD20, CD79A, and PAX5, consistent with a more favorable immune milieu and improved clinical outcomes [102]. Integrating radiomic features such as Dmax with genomic profiling provides a more

comprehensive view of cHL biology by linking tumor morphology and metabolic burden with underlying molecular and immune characteristics. This radiogenomic approach helps elucidate the biological mechanisms driving disease progression and treatment resistance, while also emphasizing the potential of Dmax as a simple, reproducible, and clinically applicable metric to refine risk stratification and support personalized therapeutic decision-making in cHL.

Molecular profiling and biomarkers

Molecular profiling has substantially advanced the understanding of Hodgkin lymphoma, revealing genomic, transcriptomic, and epigenomic alterations that not only drive disease biology but also influence clinical behavior and outcomes. Among these approaches, gene expression profiling (GEP) has been particularly impactful, providing critical insights into both the malignant Hodgkin and Reed–Sternberg (HRS) cells and the surrounding tumor microenvironment (TME). Early GEP studies demonstrated that HRS cells originate from mature B cells that have largely lost their canonical B-cell transcriptional program, while selectively upregulating genes involved in cell survival, immune modulation, and resistance to apoptosis, largely through constitutive activation of the NF-κB and JAK/STAT pathways [15,103]. Beyond tumor-intrinsic features, molecular profiling has been pivotal in dissecting the complex cellular and immune architecture of the TME in HL. These analyses have shown that HRS cells actively shape their microenvironment by overexpressing chemokines and immune checkpoint ligands, such as PD-L1 and PD-L2, thereby recruiting immunosuppressive immune subsets and fostering a niche that promotes immune escape, tumor growth, and disease persistence [19,104]. More recently, advances in high-throughput technologies—most notably single-cell RNA sequencing (scRNA-seq)—have further refined this understanding. In contrast to bulk GEP, scRNA-seq enables the dissection of transcriptional programs at single-cell resolution, revealing previously unrecognized heterogeneity within both malignant and non-malignant cell populations. This approach has provided unprecedented insight into the functional diversity, spatial organization, and dynamic interactions of immune and stromal cells within the HL TME, deepening our understanding of disease biology and uncovering potential prognostic markers and therapeutic targets. This has enabled the identification of distinct subpopulations of macrophages and T cells that actively contribute to immune escape mechanisms and resistance to therapy [42,105]. The integration of GEP with other high-throughput technologies for biomarker discovery has yielded important prognostic and predictive insights. In particular, immune-

related gene expression signatures—especially those reflecting macrophage and T-cell infiltration—have consistently emerged as strong correlates of clinical outcome in HL [106,107]. Among these, macrophage-associated markers show robust prognostic relevance, with higher expression levels being associated with inferior survival outcomes [39,108].

Molecular profiling studies have also identified thymus- and activation-regulated chemokine (TARC), also known as CCL17, as a clinically meaningful biomarker in cHL. TARC plays a central role in mediating interactions between HRS cells and the TME, particularly by shaping T-cell responses. By binding to the CC chemokine receptor 4 (CCR4), which is predominantly expressed on regulatory T cells (Tregs) and Th2-polarized CD4+ T cells, TARC promotes the recruitment of CCR4-positive T cells into the TME. This process contributes to the formation of the characteristic T-cell "rosettes" surrounding HRS cells, which deliver essential survival and proliferative signals and facilitate immune evasion [109].

Importantly, TARC is produced at high levels by malignant HRS cells, and elevated serum TARC (sTARC) concentrations have been detected years before clinical disease onset [110]. sTARC levels strongly correlate with tumor burden, disease stage, and treatment response, making it a promising biomarker for prognostic risk stratification and dynamic monitoring of therapeutic efficacy. Its utility appears particularly enhanced when combined with functional imaging modalities such as PET [111,112,113].

Despite the wealth of data generated by GEP studies, the translation of these findings into validated prognostic tools at diagnosis remains incomplete, particularly within intensive or response-adapted treatment paradigms [114,115,116]. Moreover, predictive models derived from molecular profiling require further validation in relapsed and refractory cHL populations before they can be reliably integrated into routine clinical practice [106,117]. Recent advances in liquid biopsy technologies have substantially enhanced the study of cHL, a disease historically difficult to investigate at the molecular level because of the extreme scarcity of HRS cells in tumor biopsies. The analysis of circulating tumor DNA (ctDNA), released into the bloodstream by HRS cells, now enables comprehensive genomic and transcriptomic profiling in a minimally invasive manner. In cHL, ctDNA is frequently detected at high levels and can constitute a surprisingly large proportion of total circulating cell-free DNA, exceeding expectations based on the very low tumor cell content in tissue samples. This apparent paradox is thought to reflect the high cellular turnover of HRS cells, which undergo rapid proliferation coupled with frequent apoptosis and necrosis, resulting in abundant release of tumor-derived DNA into the circulation 118. As a result, ctDNA analysis allows the sensitive detection of recurrent genomic alterations affecting key pathogenic pathways, including NF-κB (e.g., TNFAIP3 mutations), JAK/STAT

(e.g., STAT6 and SOCS1), and immune evasion mechanisms (e.g., B2M loss). Moreover, serial ctDNA monitoring provides a dynamic measure of tumor burden, with rapid declines in ctDNA levels following chemotherapy initiation correlating strongly with treatment response. These findings support the emerging role of ctDNA as a tool for minimal residual disease (MRD) assessment and early response evaluation [118,119,120,121]. Beyond its prognostic value, ctDNA profiling has also revealed biologically distinct molecular subtypes of cHL with potential therapeutic implications. In a large study by Alig et al., ctDNA from more than 300 patients identified two major genetic clusters, termed H1 and H2, each defined by distinct mutational landscapes, transcriptional programs, and clinical outcomes. H1 tumors were enriched for mutations activating the NF-κB, JAK/STAT, and PI3K pathways, whereas H2 tumors showed a higher burden of copy number alterations and were associated with a more pronounced immune infiltrate. These findings demonstrate that ctDNA-based profiling can uncover previously unrecognized biological heterogeneity in cHL and may ultimately inform risk stratification and treatment selection [122]. A recent investigation by Heger and colleagues analyzed circulating tumor DNA (ctDNA) from 243 patients enrolled in multiple pivotal trials conducted by the German Hodgkin Study Group (GHSG), with independent validation performed in an additional cohort of 96 patients treated within the EuroNet-PHL-C2 study. On the basis of these data, the authors proposed a biologically informed classification of classical Hodgkin lymphoma (cHL) comprising three distinct molecular subtypes. The *inflammatory immune-escape* subtype is characterized by recurrent copy number alterations, including amplifications of the PD-L1 locus, and by a markedly inflamed tumor microenvironment. The *virally driven* subtype is frequently associated with Epstein–Barr virus (EBV) or human herpesvirus 6 (HHV-6) infection and is defined by a highly inflammatory TME in the context of a low tumor mutational burden (TMB). In contrast, the *oncogene-driven* subtype is distinguished by recurrent mutations in genes such as *TNFAIP3*, *ITPKB*, and *SOCS1*, a relatively immunologically "cold" microenvironment, and a higher TMB. In an event-enriched validation cohort of 72 patients, these molecular subtypes were associated with significantly different progression-free survival (PFS) outcomes. Notably, the integration of ctDNA-based minimal residual disease (MRD) assessment further enhanced risk stratification, allowing the identification of patients at particularly high risk of relapse within each biological subtype [123].

Despite the substantial promise of ctDNA analysis, several obstacles must be overcome before its routine implementation in clinical practice. Chief among these is the need for rigorous standardization of pre-analytical and analytical workflows, including sample collection, ctDNA extraction, sequencing platforms, and data interpretation, to ensure reproducibility and clinical

robustness. Furthermore, large-scale prospective, multicenter studies are required to validate ctDNA-derived biomarkers and to clearly define their role in guiding therapeutic decisions in Hodgkin lymphoma.

In conclusion, the integration of advanced molecular profiling approaches, such as ctDNA analysis, with established clinical and imaging parameters represents a powerful strategy to refine risk stratification and advance personalized treatment in cHL. By uncovering molecular determinants of treatment resistance and relapse, these approaches have the potential to optimize the use of targeted therapies, including immune checkpoint inhibitors, and to further improve risk-adapted therapeutic strategies.

Aim of the study

Classical Hodgkin lymphoma (cHL) is characterized by a high cure rate; however, a clinically relevant proportion of patients develops primary refractory disease or experiences early relapse, conditions associated with poor prognosis and limited therapeutic options. Current risk stratification models, largely based on clinical and laboratory parameters, are insufficient to fully capture the biological heterogeneity of the disease and to accurately identify high-risk patients at diagnosis.

From a biological standpoint, cHL represents a unique malignancy in which a small number of neoplastic Hodgkin and Reed–Sternberg (HRS) cells are embedded within a complex and highly reactive TME. While previous studies have described the functional properties of both HRS cells and the surrounding immune infiltrate, the reciprocal interactions between these compartments and their relative contribution to clinical aggressiveness remain incompletely understood. In particular, it is still unclear to what extent disease progression is driven by intrinsic features of malignant HRS cells as opposed to the composition and functional state of the tumor microenvironment.

In this context, the present study was designed to dissect the interplay between malignant HRS cells and the tumor microenvironment, with the aim of defining their respective roles in shaping disease behavior and clinical outcome. To achieve this, we applied a spatially resolved transcriptomic approach to characterize and directly compare gene expression profiles across distinct cellular compartments, including HRS cells and key components of the immune microenvironment.

Building on these biological insights, we further sought to integrate transcriptomic data with conventional clinical parameters and radiomic features, including total metabolic tumor volume (TMTV), total lesion glycolysis (TLG), and Dmax, in order to translate microenvironmental characterization into a clinically meaningful prognostic framework. In particular, this approach enabled the development and validation of a gene-expression–based model aimed at improving risk stratification and predicting progression-free survival.

Materials and Methods

Study Design and Patients

Eligibility criteria included age between 18 and 65 years, any disease stage at diagnosis, and treatment with systemic chemotherapy regimens, such as ABVD or related protocols, including BV-AVD. Additional inclusion requirements were the availability of formalin-fixed, paraffin-embedded (FFPE) diagnostic tissue suitable for gene expression analyses and a minimum follow-up of six months from diagnosis. Two independent cohorts of patients with histologically confirmed classical Hodgkin lymphoma (cHL) diagnosed between 2007 and 2023 were analyzed. The first cohort consisted of a retrospective, single-center series of 155 patients treated at the AUSL–IRCCS of Reggio Emilia. The second cohort comprised a retrospective, multicenter series of 89 patients enrolled from nine Italian Hematology Units, including AUSL–IRCCS of Reggio Emilia, Fondazione IRCCS Policlinico San Matteo (Pavia), San Giovanni Moscato Hospital (Avellino), Veneto Oncology Institute (Padova), AUSL of Piacenza, Azienda Ospedaliera Santa Maria of Terni, and Hematology Units in Torino. All diagnostic samples were centralized at the AUSL–IRCCS of Reggio Emilia for centralized processing and analysis.

The primary study endpoint was progression-free survival (PFS), defined as the interval from the date of diagnosis to disease relapse, progression, or death from any cause, whichever occurred first. The study was conducted in accordance with the Declaration of Helsinki and received approval from the institutional review board. Written informed consent was obtained from all living patients still under active follow-up at our institution after comprehensive explanation of the study objectives and procedures.

Spatial Transcriptomics analysis

Spatial transcriptomic profiling was performed using the GeoMx DSP® (Nanostring technologies, USA) on 5 μm FFPE tumor tissue sections. We analyzed samples from eight patients, including four classified as relapsed/refractory (R/R+) and four non-relapsed (R/R-), based on a minimum follow-up of three years. Slides were hybridized with the GeoMx® Cancer Transcriptome Atlas panel according to manufacturer's protocol. For target retrieval, slides were incubated in 1X Tris-EDTA buffer (pH 9.0) for 10 minutes, followed by treatment with Proteinase K 1μg/ml for 10 minutes. In situ hybridization with the RNA probe mix was

conducted overnight. For spatial selection, slides were stained with the following reagents: a primary antibody against CD30 (clone 130M96, Sigma-Aldrich), followed by a secondary antibody (A-21235, ThermoFisher) for HRS cell identification; a primary antibody against CD45 (NBP2-34528-AF532, Novus) to visualize the immune tumor microenvironment; a primary antibody against CD20 (NBP2-47840-AF594) to detect non-tumoral B cells; and the nuclear stain SYTO-13 (GMX-MORPH-NUC-12, Nanostring Technologies, USA). Three types of area of illumination (AOIs) were defined based on morphology markers: (i) HRS regions (CD30+, CD45+, CD20-, SYTO-13+), (ii) peritumoral immune microenvironment (CD30-, CD45+, CD20-, SYTO-13+) and (iii) non-tumoral Bcells (CD30-, CD20+, CD45+, SYTO-13+). Hybridized RNA probes were collected from the selected AOIs, and sequencing libraries were generated using the GeoMx® Seq Code Pack (Nanostring technologies). Libraries were pooled together, purified by AMPure XP beads (Beckman Coulter, Brea, California, USA) clean up and resuspended in a volume proportional to the number and dimension of pooled AOIs. The quality of library pools was evaluated by Agilent Bioanalyzer. Libraries were quantified by Qubit High Sensitivity kit (Thermo Scientific) diluted to 1.6pM and sequenced by NextSeq 500 (paired-end 2 × 27), expecting for each library/AOI a coverage of at least 40 reads per μm2 of collected region. Following demultiplexing, FastQ files were converted to DCC format by GeoMx® Next-generation sequencing (NGS) Pipeline App (BaseSpace Illumina Sequence Hub) and uploaded on the GeoMx DSP platform for association with corresponding AOIs. Data analysis was performed using the GeoMx DSP analysis suite. Quality control (QC) tests were first applied to the AOIs to evaluate sequencing quality parameters, including raw reads (>1000), aligned reads (>80%), sequencing saturation (>50%), and background effects (no-template control counts <1000). Probe-level QC was then carried out according to the standard instrument parameters, and all genes passing QC were retained for subsequent analyses. AOIs expressing less than 3% of genes above the limit of quantitation (LOQ; defined as two standard deviations above the background signal of negative probes) were excluded (n=31). Genes expressed above the LOQ in less than 5% of the AOIs were also removed. Raw gene counts were normalized to the third quartile (Q3) of all target genes.

After normalization, gene-expression profiles of the AOIs from the three different compartments (HRS cells, tumor microenvironment, and non-tumoral B cells) were compared between R/R+ and R/R- patients using a linear mixed model (LMM). This analysis aimed to identify differentially expressed genes (DEGs) based on the following formula: log2(gene) ~ Group + (1|Patient_ID) + (1|Patient_ID:Center). All bioinformatic analyses were conducted in R Software v4.4.0 using the packages ggplot2, pheatmap, RColorBrewer, corrplot, Biobase,

matrixStats. The density of HRS cells was calculated by dividing the area of each AOI by the surface area of the corresponding region of interest (ROI) from which it was derived.

Digital bar-coding bulk gene-expression profiling

Digital barcoding–based gene expression profiling was performed using the PanCancer Immune Profiling Panel (NanoString Technologies), as previously described [124]. Total RNA was extracted from five consecutive 5-µm FFPE tissue sections using the Maxwell® RSC RNA FFPE Kit (Promega), according to the manufacturer's instructions.

After normalization, raw gene counts were $\log_2$-transformed, and gene expression levels were correlated with progression-free survival (PFS) using a Cox proportional hazards regression model. Correlation matrices were generated using Pearson's correlation coefficient, and only statistically significant correlations ($p < 0.05$) were visualized. Comparative analyses of B-cell–related gene expression signatures were performed using the Kruskal–Wallis test.

All bioinformatic and statistical analyses were conducted using R software version 4.0.4, employing the packages survival, survminer, forestplot, and corrplot. Gene ontology (GO) enrichment analysis was performed on the Biological Process sub-ontology using the Enrichr online platform. The gene expression datasets generated and analyzed in this study are publicly available in the Gene Expression Omnibus (GEO) repository under accession numbers GSE132348 and GSE184662.

Deconvolution analysis

Cell-type deconvolution was performed using the CIBERSORTx algorithm (https://cibersortx.stanford.edu/)[125] based on a customized gene matrix (doi: 10.3324/haematol.2024.285266. PMID: 39021213; PMCID: PMC11532716). The algorithm was applied to both CD45+ AOIs obtained from spatial transcriptomic analysis and to bulk expression data generated by nCounter platform, to estimate the relative proportions of each cell types, including HRS. Absolute scores for each cell type were compared between R/R+ and R/R- AOIs, with p-values calculated using the Wilkoxon test.

Statistical analysis

For descriptive statistics, categorical variables and dichotomized continuous variables were expressed as absolute numbers and percentages for the entire cohort. PET-derived features,

including total metabolic tumor volume (TMTV) and the maximum distance between the two most distant lesions (Dmax), were dichotomized using cutoff values validated in our previous work 20. Association between clinical variables, radiomic features and cluster groups were evaluated in univariate analysis using Fisher's exact test.

The B-cell score was generated using the glmnet package in R, employing an Elastic Net penalized regression model with $\alpha = 0.1$. The model was trained on a predefined set of 18 B cell-related genes selected based on biological relevance and prior analysis. The coefficients derived from this model in the training cohort were then applied to the validation cohort gene expression dataset after normalization to the training set using the R function limma remove Batch Effect. ROC curves were designed by R package timeROC considering a follow-up period of three years.

Survival analysis was performed using the Cox proportional hazards model, and results were reported as hazard ratios (HRs) with corresponding 95% confidence intervals (95%CI) and p values based on the Wald-test. Survival curves were estimated using the Kaplan-Meier method, and comparisons between groups were made using the log-rank test. Patients who were alive and event-free were censored at the date of last follow-up. Statistical significance was set at $p \leq 0.05$. All analyses were performed using R software, version 4.0.4.

Immunohistochemistry

Immunohistochemistry was performed using an automated immunostainer (Ventana BenchMark, Tucson, AZ); 3, 3′-diaminobenzidine was used as the chromogen and Harris's hematoxylin as the counterstain.

Results

Patient Demographics and Clinical Characteristics

Table I summarizes the demographic, clinical, and laboratory characteristics of the training and validation cohorts. The training cohort included 155 patients with classical Hodgkin lymphoma, while the validation cohort comprised 89 patients.

In the training cohort, sex distribution was balanced, with 76 females (49.0%) and 79 males (51.0%). A similar distribution was observed in the validation cohort, where females accounted for 56.2% (n = 50) and males for 43.8% (n = 39). The majority of patients in both cohorts were younger than 45 years, representing 67.7% of the training cohort and 80.5% of the validation cohort.

Baseline laboratory parameters were largely comparable between cohorts. Albumin levels ≤4 g/dL were observed in 64.0% of patients in the training cohort and 59.6% in the validation cohort, although missing data were present for this variable in both datasets. Anemia, defined as hemoglobin ≤10.5 g/dL, was detected in 13.1% of patients in the training cohort and 17.9% in the validation cohort. Elevated leukocyte counts (>15 × 10^3/mm^3) were relatively uncommon, occurring in approximately 13–15% of patients across both cohorts.

Similarly, increased LDH levels (LDH/ULN >1) were documented in roughly one third of patients in both cohorts (34.9% in the training cohort and 32.0% in the validation cohort). Elevated erythrocyte sedimentation rate (ESR >50 mm/h) was present in approximately half of the training cohort (49.7%) and in 43.1% of the validation cohort, with a proportion of missing values.

Regarding disease characteristics, advanced-stage disease (IIB–III–IV) was observed in 55.5% of patients in the training cohort and 64.4% in the validation cohort. Bulky disease was relatively infrequent in both cohorts, reported in 9.7% and 11.9% of patients, respectively. Extranodal involvement was more prevalent in the validation cohort (58.4%) compared with the training cohort (38.1%).

According to the Hasenclever prognostic score, the majority of patients in both cohorts fell within the low-to-intermediate risk categories (score 0–2), accounting for 61.9% of the training cohort and 64.9% of the validation cohort. Interim PET (iPET) results were available for a subset of patients and showed a higher proportion of positive scans in the validation cohort

(40.6%) compared with the training cohort (17.6%), although missing data were substantial for this variable.

Table I. Descriptive statistics

Variable	Training cohort overall (N=155)	Validation cohort overall (N=89)
Sex		
F	76 (49.0%)	50 (56.2%)
M	79 (51.0%)	39 (43.8%)
Age		
≤45	105 (67.7%)	70 (80.5%)
>45	50 (32.3%)	17 (19.5%)
NA		2
Albumin (g/dl)		
≤4	87 (64.0%)	34 (59.6%)
>4	49 (36.0%)	23 (40.4%)
NA	19	32
Hemoglobin (g/dl)		
≤10.5	20 (13.1%)	15 (17.9%)
>10.5	133 (86.9%)	69 (82.1%)
NA	2	5
Leukocytes (cells/mm^3)		
≤15*10^3	133 (86.9%)	71 (85.5%)
>15*10^3	20 (13.1%)	12 (14.5%)
NA	2	6
LDH/ULN		
≤1	97 (65.1%)	51 (68.0%)
>1	52 (34.9%)	24 (32.0%)
NA	6	14
ESR		
≤50	74 (50.3%)	41 (56.9%)
>50	73 (49.7%)	31 (43.1%)
NA	8	17
Stage		
I-IIA	69 (44.5%)	31 (35.6%)
IIB-III-IV	86 (55.5%)	56 (64.4%)
NA		2
Bulky		
no	139 (90.3%)	52 (88.1%)
yes	15 (9.7%)	7 (11.9%)
NA	1	30
Extranodal		
no	96 (61.9%)	37 (41.6%)

Variable	Training cohort overall (N=155)	Validation cohort overall (N=89)
yes	59 (38.1%)	52 (58.4%)
HASENCLEVER		
0-1-2	96 (61.9%)	37 (64.9%)
≥3	58 (38.1%)	20 (35.1%)
NA		32
iPET		
neg	117 (82.4%)	19 (59.4%)
pos	25 (17.6%)	13 (40.6%)
NA	13	46

Spatially Informed Transcriptomic Characterization of Classical Hodgkin Lymphoma

A morphology-driven, spatially resolved transcriptomic strategy was employed to characterize gene expression patterns in HRS cells and the surrounding tumor microenvironment (TME) using lymph node specimens from a matched case–control cohort of cHL patients stratified by relapse/refractoriness (R/R− vs. R/R+) (Figure 6 A–B). Overall, 148 distinct Areas of Interest (AOIs) were analyzed, including 62 derived from $CD30^+$ HRS cells, 56 from the TME ($CD45^+/CD30^-$), and 30 from non-malignant B cells ($CD45^+/CD20^+$), which served as a reference population. Patients in the R/R+ group accounted for more than half of the AOIs across all cellular compartments, including 51% of those corresponding to HRS cells.

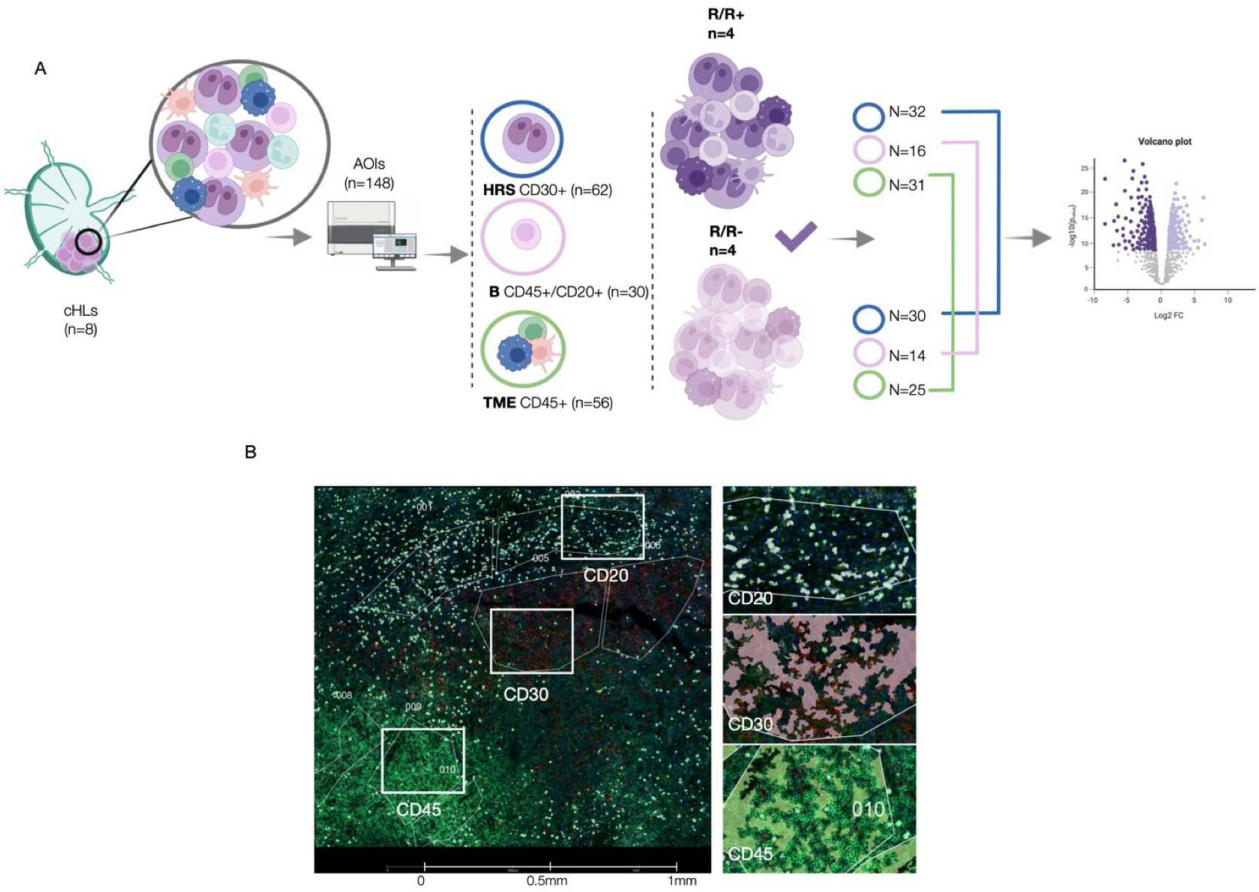

Figure 6 A) Workflow of the transcriptomic analysis. B) Representative scan of a Hodgkin Lymphoma excisional biopsy processed using GroMx® DSP. The outlined areas indicate the regions of interest (ROIs), while the highlighted area represent the actual areas of illumination (AOIs) collected: red mask for HRS cells, green mask for the immune tumor microenvioronment (TME), and yellow mask for the non tumoral B cells.

Aggressive Classical Hodgkin Lymphoma Is Defined by Unique Transcriptional Programs

Unsupervised clustering of transcriptomic profiles derived from HRS-associated AOIs revealed a marked association with clinical outcome. In particular, Cluster II was predominantly composed of samples from relapsed/refractory patients, encompassing 96.8% of R/R+ AOIs, whereas Cluster I was enriched for R/R− cases, which accounted for 73.3% of the corresponding AOIs (Figure 7A). Comparative transcriptomic analysis between R/R+ and R/R− HRS-AOIs identified 212 genes displaying differential expression (Figure 7B), of which 20 were significantly overexpressed in the R/R+ group. Functional enrichment analysis indicated that these genes were mainly involved in tumor-promoting biological processes, including apoptotic resistance and angiogenic signaling, and further highlighted the

contribution of NF-κB pathway activation (Figure 7C). Among these, CCL17 (TARC) and IL13—cytokines implicated in immune suppression and HRS cell proliferation in cHL—were notably upregulated in the R/R+ samples (Figure 7D).

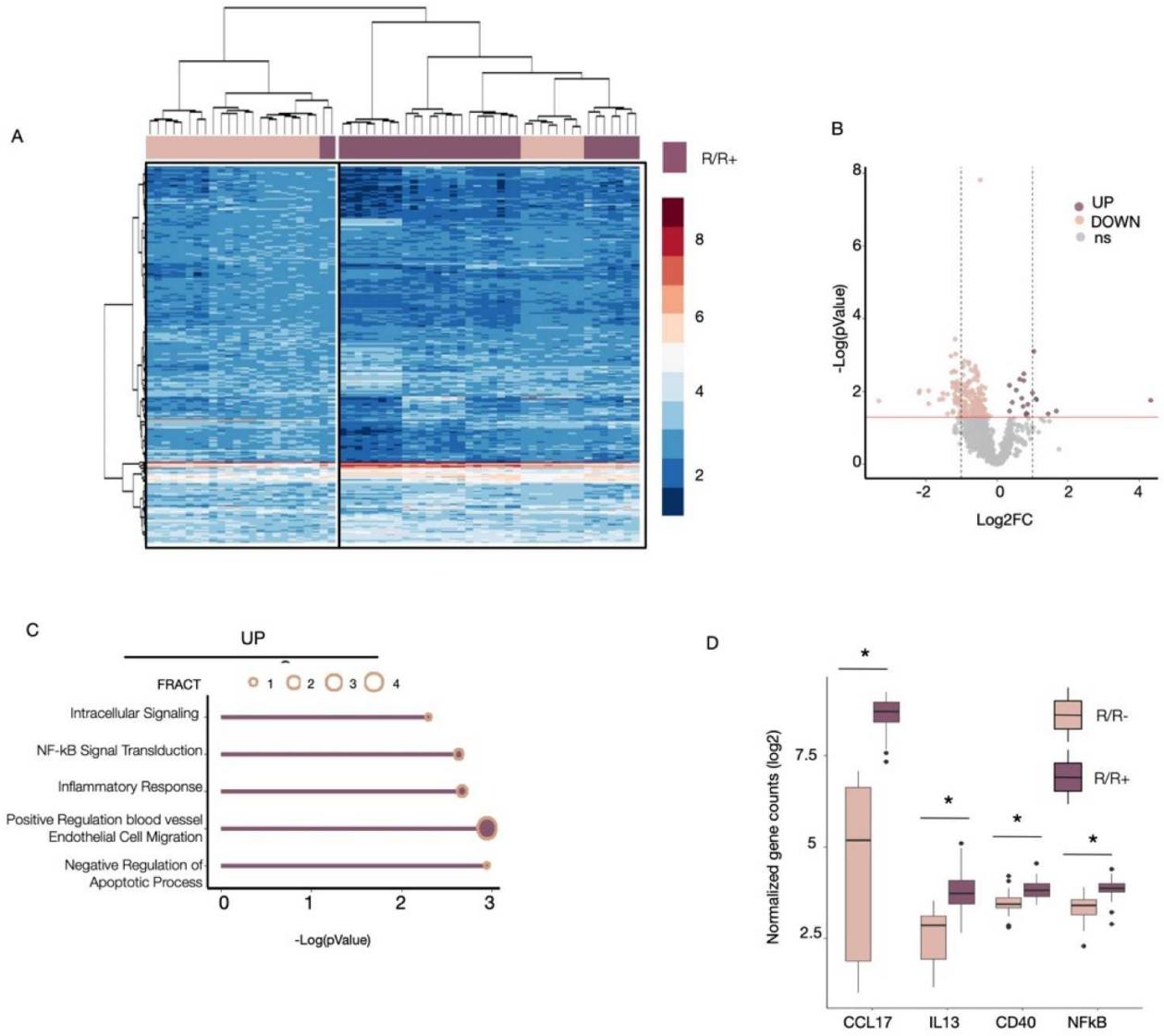

Figure 7 A) Unsupervised clustering including HRS AOIs collected from biopsies of R/R- and R/R+ patients. B) Volcano plot showing differentially expressed genes (DEGs) between HRS AOIs of R/R+ and R/R- patients. Violet dots represent genes significantly up-regulated, and pink dots represent genes significantly down-regulated in R/R+ samples. DEGs were considered significant at $p \leq 0.05$. C) Gene Ontology (GO) analysis of biological processes associated with up-regulated genes in HRS AOIs of R/R+ patients. The fraction of deregulated genes enriched in each pathway is shown; p-values were calculated using Fisher's exact test. D) Boxplot showing the most relevant up-regulated genes in HRS-AOIs from R/R+ samples. pValues were calculated by LMM and considered significant for $p \leq 0.05$.

In contrast to the limited number of upregulated transcripts, a substantially larger set of 192 genes was found to be significantly downregulated in aggressive cHL samples. Functional enrichment analyses revealed that these genes were predominantly involved in immune-activating pathways, including chemokine-mediated paracrine signaling, exemplified by CXCL9 and CXCL10, as well as Type I interferon (IFN-I) signaling cascades (Figure 8A–B). Consistently, key transcriptional regulators downstream of IFN-I signaling, namely STAT1 and STAT2—previously shown to exert growth-restrictive effects on HRS cells—were markedly reduced in aggressive cases (Figure 8B). The diminished activity of these factors, particularly STAT1, is known to relieve antagonism of STAT6-driven signaling, thereby favoring HRS cell survival and proliferation. In addition, aggressive samples exhibited reduced expression of genes involved in the DNA damage response, including ATM and ATR, as well as multiple chromatin-associated regulators (Figure 8B). Collectively, these findings indicate that HRS cells from R/R+ and R/R− patients are characterized by profoundly distinct transcriptional programs, reflecting both intrinsic cellular adaptations and altered paracrine interactions that contribute to disease progression.

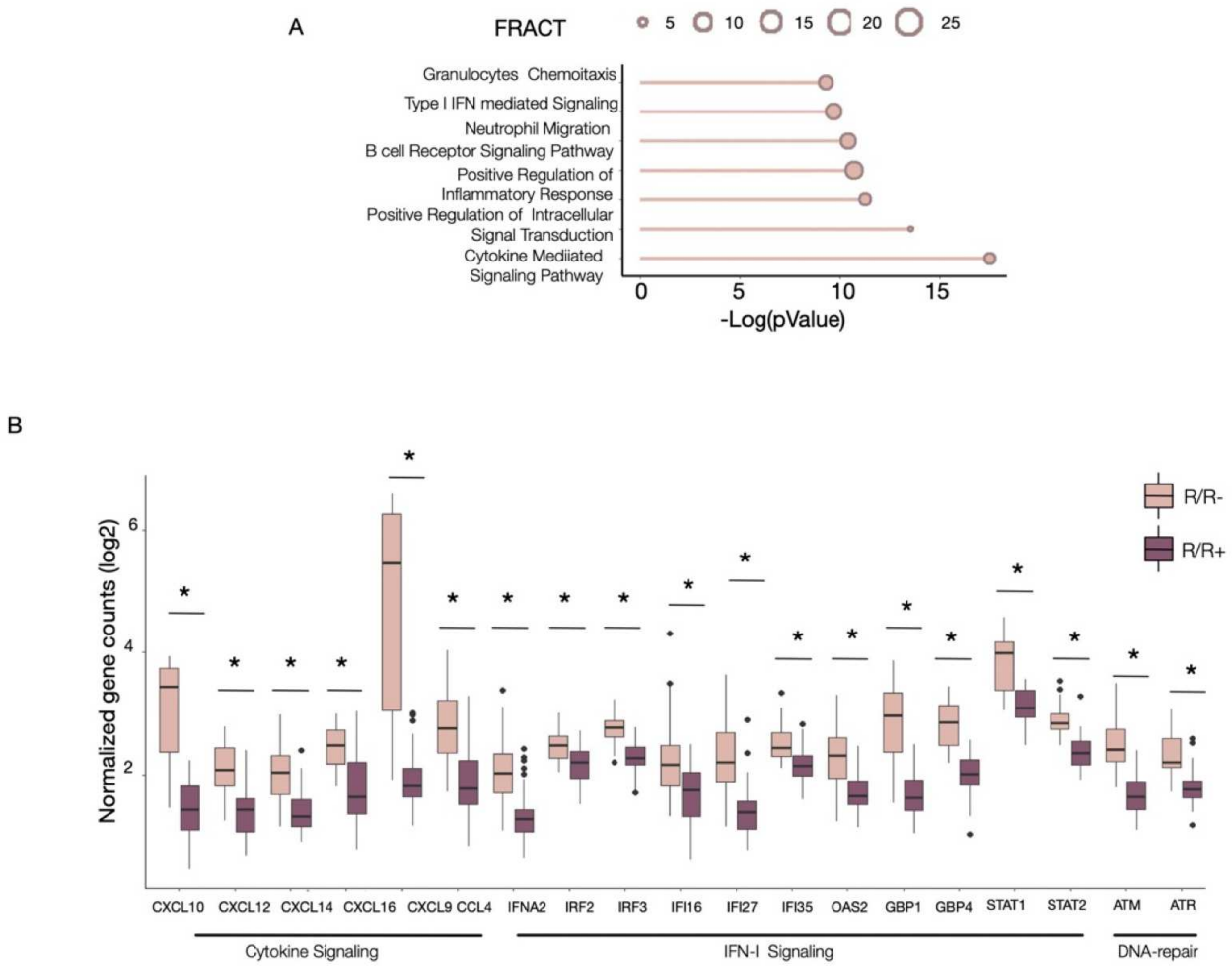

Figure 8. A) GO analysis of biological processes associated with down-regulated genes in HRS AOIs of R/R+ patients. The fraction of deregulated genes enriched in each pathway is shown; p-values were calculated using Fisher's exact test. B) Boxplot showing the most relevant down-regulated genes in HRS-AOIs from R/R+ samples. p-values were calculated by LMM and considered significant for $p \leq 0.05$.

Immune Dysregulation of the Tumor Microenvironment in Aggressive Classical Hodgkin Lymphoma

Transcriptomic profiling of tumor microenvironment–derived Areas of Interest (TME-AOIs) revealed pronounced differences between aggressive (R/R+) and treatment-responsive (R/R−) cHL cases (Figure 9A). A total of 115 genes exhibited differential expression, with 47 transcripts upregulated and 68 downregulated in aggressive lesions. Functional annotation of these changes pointed to a substantial disruption of adaptive immune responses, in line with the immunosuppressive phenotype characteristic of aggressive disease. Notably, the B-cell compartment emerged as one of the most profoundly affected components of the TME (Figure 9B). Genes involved in key B-cell functions, including proliferation, chemotactic signaling, and

differentiation, were markedly reduced. Consistently, aggressive tumors displayed decreased expression of B-cell–specific markers (Figure 9C) as well as multiple MHC class II molecules, suggesting a compromised capacity for B-cell–mediated antigen presentation (Figure 9D).

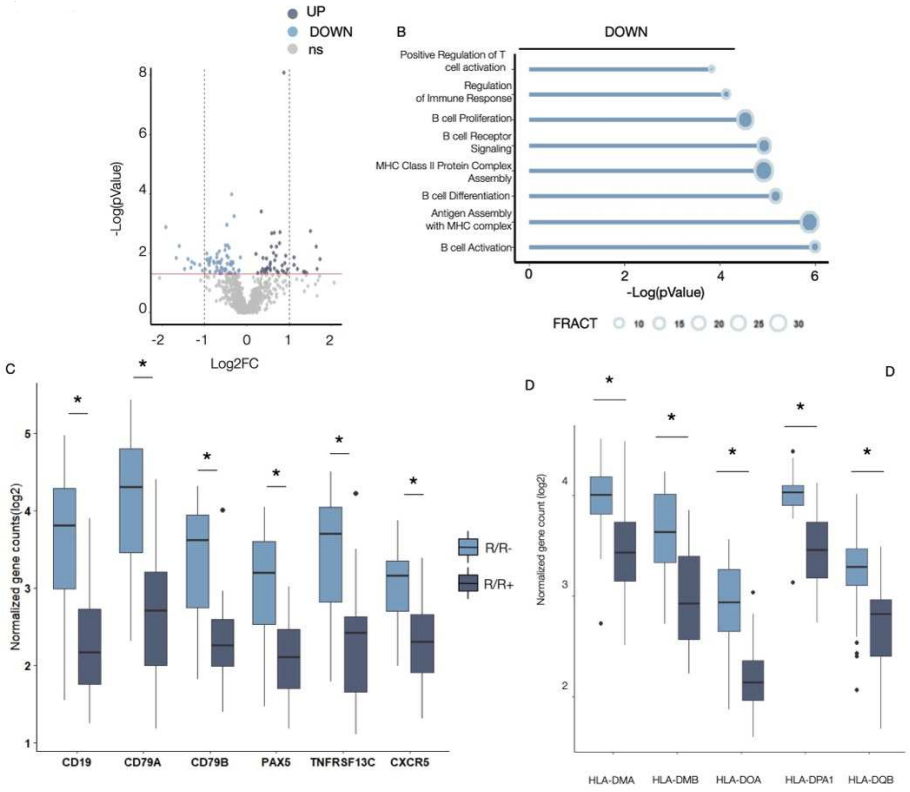

Figure 9. A) Volcano plot showing differentially expressed genes (DEGs) between TME AOIs of R/R+ and R/R- patients. Blue dots represent genes significantly up-regulated, and light blued dots represent genes significantly down-regulated in R/R+ samples, DEGs were considered significant at $p \leq 0.05$. B) GO analysis of biological processes associated with down-regulated genes in TME AOIs of R/R+ patients. The fraction of deregulated genes enriched in each pathway is shown; p-values were calculated using Fisher's exact test. C-D) Boxplot showing relevant down-regulated genes in TME-AOIs from R/R+ samples. C) B cells lineage markers. D) MCH-II genes. pValues were calculated by LMM and considered significant for $p \leq 0.05$.

Genes overexpressed in TME-AOIs from aggressive cHL cases delineated a tumor microenvironment skewed toward immune evasion (Figure 10A). In particular, transcriptomic changes indicated an enrichment of macrophage-related signatures, with a marked increase in markers characteristic of alternatively activated, M2-like macrophages, including CD63 and CSF1R (Figure 10B), a population known to support tumor progression and suppress anti-tumor immunity. In parallel, the expression of key immune checkpoint–related genes, such as VSIR (encoding VISTA) and SIRPA, was significantly elevated, further reinforcing an

immunosuppressive milieu (Figure 10C). Additionally, genes implicated in extracellular matrix interaction and remodeling were upregulated (Figure 10D). Notably, both matrix remodeling processes and VISTA signaling have been reported to favor M2 macrophage polarization. Consistent with this immune-evasive phenotype, the chemokine CCL17—previously associated with adverse clinical outcomes—was also significantly increased, supporting the existence of a reinforcing crosstalk between malignant cells and the tumor microenvironment (Figure 10C).

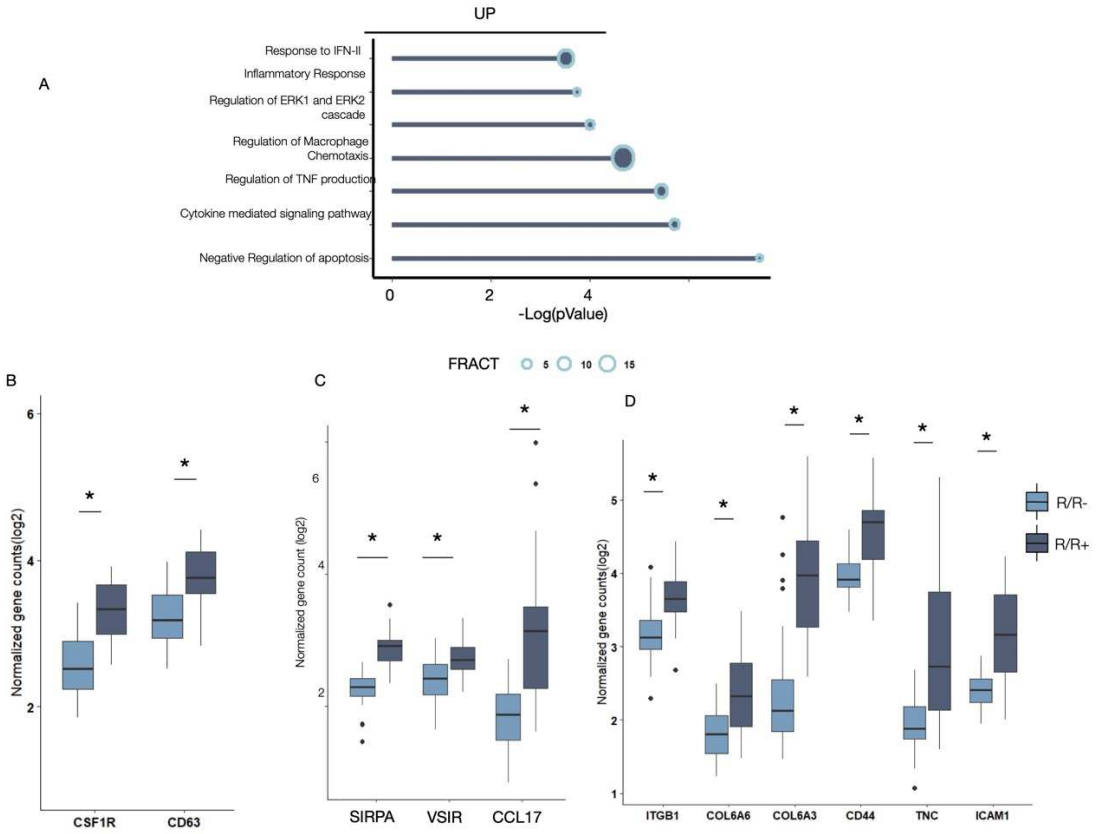

Figure 10. A) Gene Ontology (GO) analysis of biological processes associated with up-regulated genes in TME AOIs of R/R+ patients. The fraction of deregulated genes enriched in each pathway is shown; p-values were calculated using Fisher's exact test. B-D) Boxplot showing the relevant up-regulated genes in TME-AOIs from R/R+ samples. B) Macrophages markers. C) Immune Checkpoints. D) Matrix remodeling. pValues were calculated by LMM and considered significant for $p \leq 0.05$.

Immune Cell Composition Analysis Indicates Immunosuppressive Rewiring

Cell-type deconvolution analysis, aimed at estimating the relative abundance of immune populations, provided further evidence of extensive remodeling of the tumor microenvironment in R/R+ cHL lesions (Figure 11A). Aggressive samples displayed a significant expansion of

immunosuppressive cell populations, including regulatory T cells and mast cells, accompanied by functional reprogramming of key immune subsets. Notably, macrophages exhibited a shift from a pro-inflammatory M1 phenotype toward a tumor-supportive M2 state, while natural killer cells transitioned from an activated to a resting, less cytotoxic profile. In parallel, a pronounced contraction of the non-malignant B-cell compartment was observed, affecting both naïve and memory subsets, together with a reduction in T follicular helper cells. This pattern is consistent with the previously observed loss of B-cell MHC class II expression and further supports the impairment of B-cell–mediated immune functions in aggressive disease.

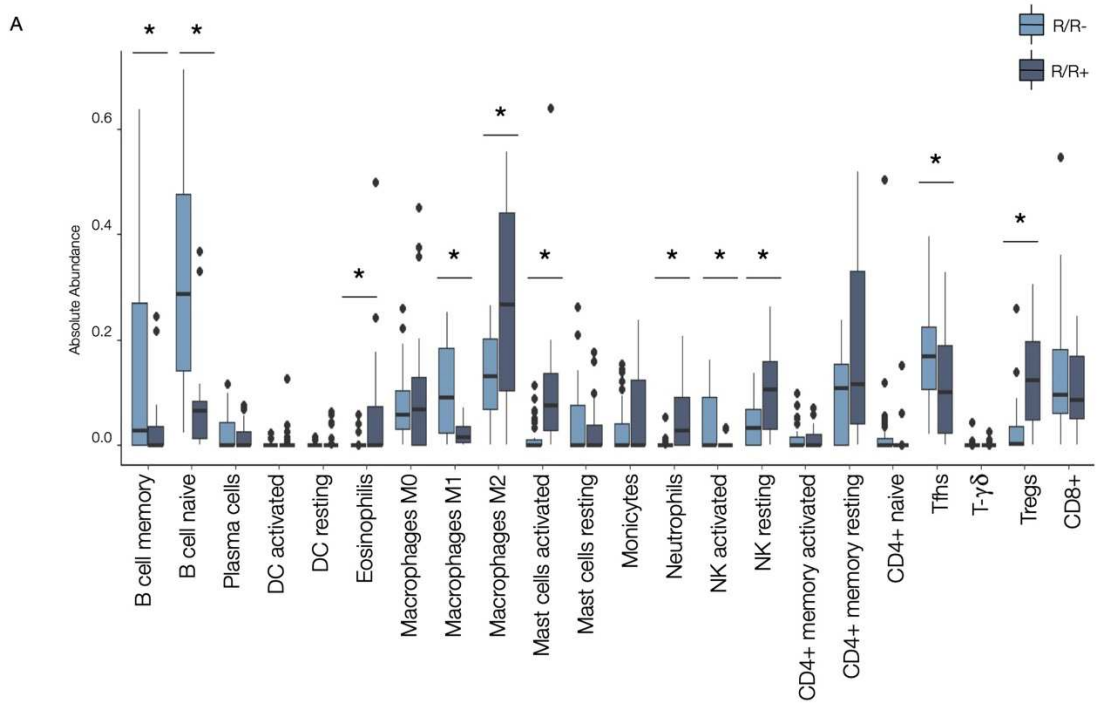

Figure 11. A) TME deconvolution results showing the mean absolute abundance of each cell population across all AOIs in R/R+ and R/R− samples. Statistical significance was assessed using the Wilcoxon test. Comparisons were considered significant at $p \leq 0.05$.

Dynamic Interplay Between Immune Activation and Immune Suppression

Correlation analyses highlighted the tightly interconnected nature of the observed shifts in immune cell populations within the tumor microenvironment (Figure 12A). Naïve B cells exhibited a strong inverse relationship with immunosuppressive subsets that were expanded in aggressive disease, including regulatory T cells, mast cells, resting natural killer cells, and M2-polarized macrophages, while showing a positive association with activated NK cells. Conversely, M2 macrophages were negatively correlated not only with naïve B cells but also with T follicular helper cells and activated NK cells. These relationships are visually

summarized in the radar plot shown in Figure 12B, which illustrates a clear dichotomous segregation between immune-active and immune-suppressive cell populations within the TME, further emphasizing the opposing distribution of non-malignant B cells relative to immune-evasive cellular compartments.

Normal B Cells as Modulators of Tumor Aggressiveness

Collectively, these findings support a model in which non-malignant B cells exert an active restraining effect on the aggressive behavior of HRS tumor cells. Aggressive (R/R+) cHL lesions were consistently characterized by an increased density of HRS cells accompanied by a marked depletion of normal B cells within the tumor microenvironment (Figure 12C). Notably, the loss of non-tumoral B cells emerged as a more critical determinant of clinical aggressiveness than tumor burden alone. Lesions with comparable HRS cell content were classified as R/R− or R/R+ primarily on the basis of the estimated abundance of normal B cells, irrespective of overall tumor load (Figure 12D). These observations indicate that the maintenance of a dense, protective population of non-malignant B cells within the TME attenuates HRS-driven aggressiveness and limits the development of an immunosuppressive tumor milieu.

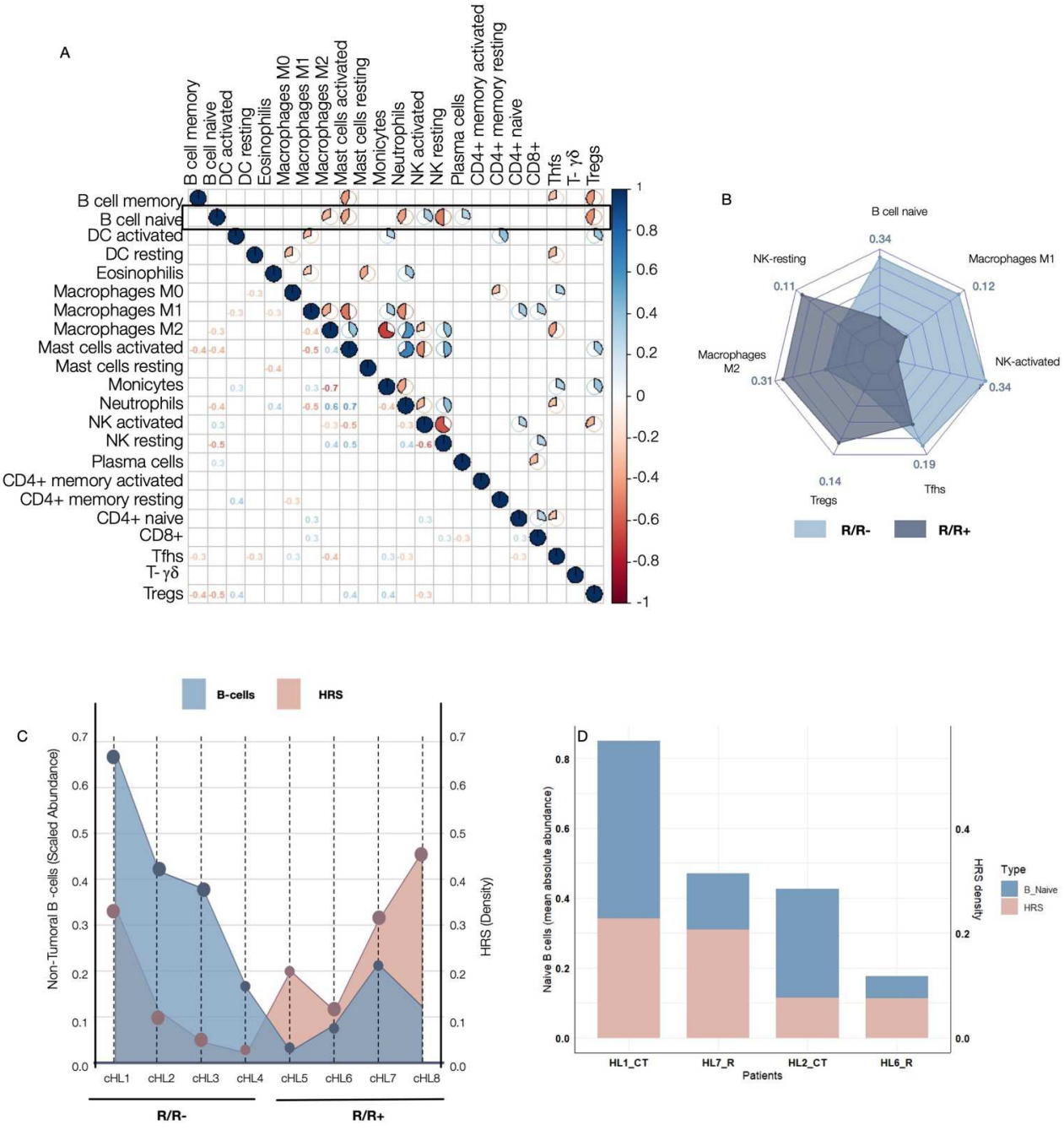

Figure 12. A) Correlation matrix of immune cell populations derived from the deconvolution analysis. Correlation coefficients are shown using a color gradient: red indicates negative correlations, and blue indicates positive ones. Only statistically significant correlations are displayed ($p \leq 0.05$). B) Radar plot showing the relationship between significantly correlated cell populations in R/R+ and R/R− samples. C–D) Histogram showing HRS cell density, calculated as the mean ratio of HRS-AOI to the corresponding ROI for each patient (right y-axis), and the mean absolute abundance of naïve B cells derived from deconvolution analysis of TME AOIs (left y-axis).

HRS Cell Reprogramming and Loss of B-Cell Identity

Although Hodgkin and Reed–Sternberg (HRS) cells derive from B lymphocytes, they undergo extensive transcriptional reprogramming that leads to a partial or near-complete loss of B-cell identity. The degree of this phenotypic transdifferentiation appears to be closely linked to clinical aggressiveness. Based on this premise, we hypothesized that the aggressive behavior observed in R/R+ lesions reflects a more advanced transdifferentiation state.

Consistent with this hypothesis, principal component analysis (PCA) revealed a continuous transcriptional trajectory spanning from normal $CD20^+$ B cells to HRS cells (Figure 13A). HRS cells from R/R+ lesions occupied the most distant position from normal B cells, indicative of a profound erosion of B-cell lineage features, whereas HRS cells from R/R− cases localized to an intermediate transcriptional state. In line with these findings, expression of canonical B-cell lineage markers progressively declined along this continuum, reaching the lowest levels in the most aggressive HRS cells (Figure 13 B–C). Notably, HRS cells from R/R+ lesions uniquely exhibited marked upregulation of CCL17 and IL13, suggesting that the acquisition of immunosuppressive signaling properties intensifies as B-cell identity is progressively lost.

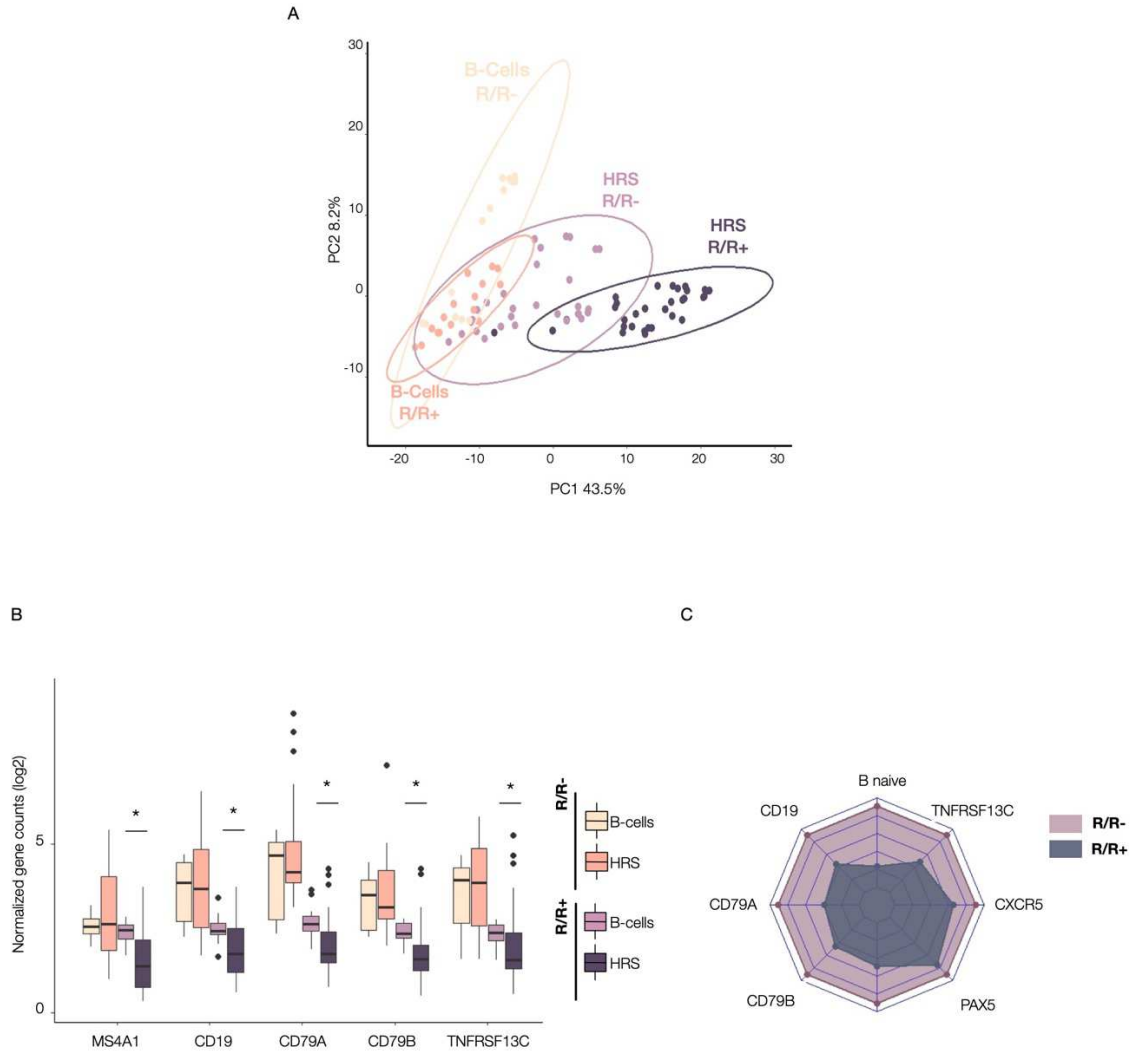

Figure 13. A) Principal Component Analysis (PCA) shows the variance of DEGs obtained by comparing HRS AOIs and non-tumoral B cells AOIs in R/R+ and R/R− samples. B) Boxplot showing the expression of B cell lineage genes in non-tumoral B cells and HRS cells from R/R+ and R/R− samples. p-values were calculated using Dunn's test and considered significant at $p \leq 0.05$. C) Radar plot showing the relationship between the abundance of naïve B cells, derived from the deconvolution analysis of TME AOIs, and the expression of B cell lineage genes in HRS AOIs from R/R+ and R/R− samples.

Notably, differential transcriptomic analysis of the CD20⁺ non-malignant B-cell compartment revealed only minimal differences between R/R+ and R/R− lesions, with samples clustering together independently of clinical outcome (Figure 14A–B). Collectively, these findings support a model in which disease progression is primarily driven by the degree of B-cell identity loss in HRS cells. Importantly, the preservation of a dense population of normal, protective B cells within the tumor microenvironment appears to constrain this reprogramming process, thereby attenuating tumor aggressiveness and limiting the development of an immunosuppressive milieu.

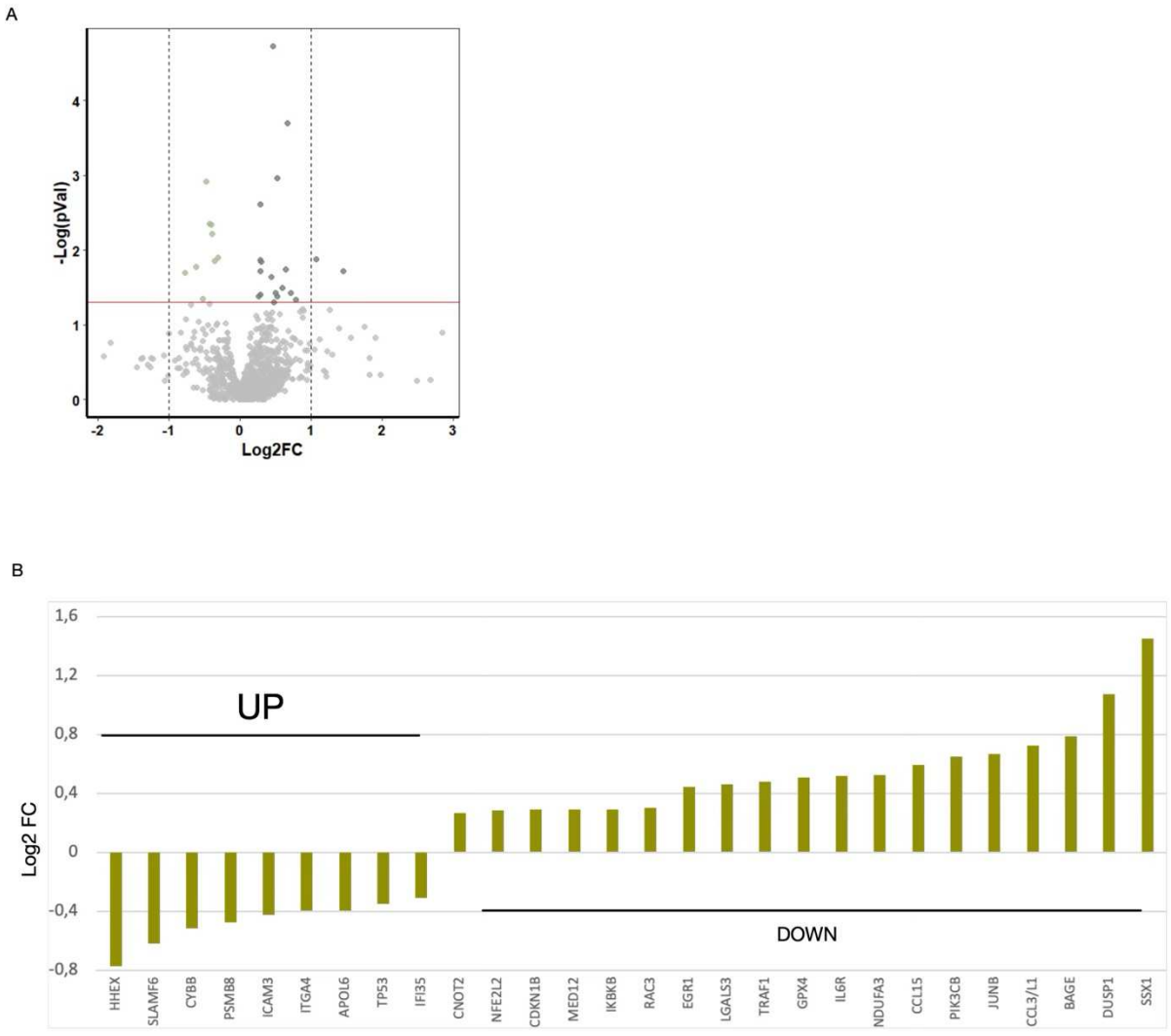

Figure 14. A) Volcano plot showing differentially expressed genes (DEGs) between CD20+ AOIs of R/R+ and R/R− patients. Green dots represent genes significantly upregulated, and light green dots represent significantly down-regulated in R/R+ samples. DEGs were considered significant at $p \leq 0.05$. B) Boxplot showing all deregulated genes in CD20+ AOIs from R/R+ samples. p-values were calculated by LMM and considered significant for $p \leq 0.05$.

Sustained Non-Malignant B-Cell Presence Predicts Favorable Progression-Free Survival

To validate and extend these observations in a larger cohort, we analyzed the expression of a curated panel of 770 immune-related genes using digital barcoding technology in a retrospective, single-center series of 155 cHL patients serving as a training cohort (Figure 15A; Table I). Gene expression levels were correlated with progression-free survival (PFS) to identify molecular features associated with clinical aggressiveness. Baseline patient characteristics are summarized in Table I. The estimated 4-year PFS for this cohort was 80.4% (95% CI, 74.1–87.3) (Figure 15B).

Following quality control and data normalization, Cox proportional hazards regression was applied to identify transcripts significantly associated with PFS. This analysis identified 101 genes with prognostic relevance. Among these, 66 genes were positively associated with PFS, indicative of a favorable clinical outcome (Figure 15D). Functional enrichment analyses revealed that these protective genes were predominantly involved in pathways related to B-cell activation and regulation (Figure 15D and Figure 16B). In contrast, 41 genes were inversely correlated with PFS and associated with adverse outcomes (Figure 16A), mapping primarily to broader immune-related processes (Figure 16B–C).

Focusing on the protective gene set, correlation network analysis identified a tightly interconnected core of 22 genes (Figure 15D). Notably, 18 of these genes (81.1%) corresponded to canonical markers of the non-malignant B-cell lineage, including CD20, CD19, CD79A, CD79B, and PAX5. This 18-gene panel was subsequently defined as the B-cell–derived signature (B-signature).

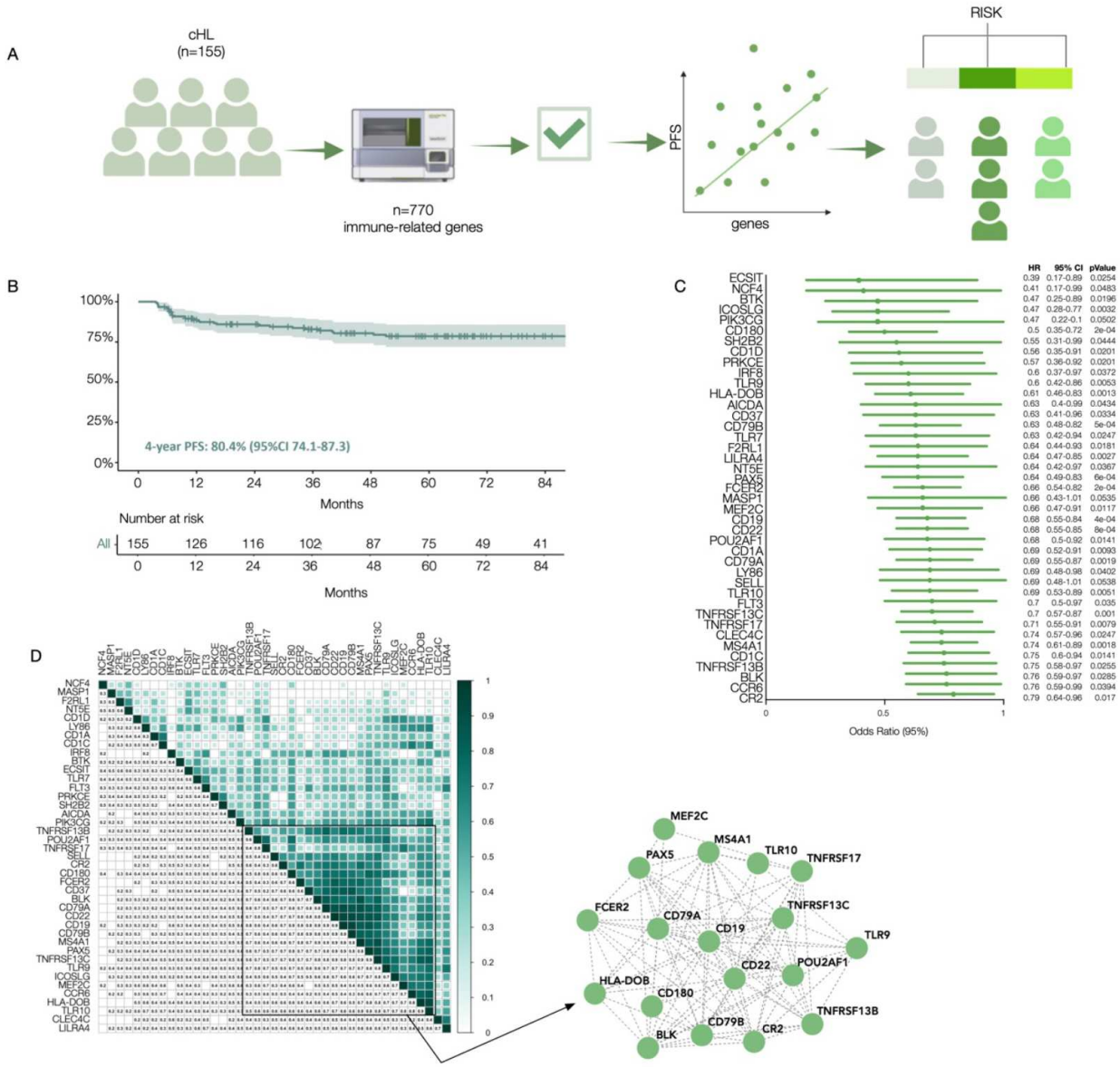

Figure 15. A) Workflow of the digital bar-coding bulk gene-expression profiling in the monocentric retrospective cohort of cHL (training). B) Kaplan–Meier curves showing progression-free survival (PFS) in the training cohort. C) Forest plot showing the results of Cox regression analysis for genes significantly associated with improved progression-free survival (PFS), indicating a protective effect. D) Correlation matrix including protective gene expression values. Correlation coefficients are shown using a green color gradient. Only statistically significant correlations are displayed ($p \leq 0.05$). Genes showing strong correlation coefficients ≥ 0.8 and biological relatedness are highlighted in the network plot. E) Unsupervised clustering including the 18 genes previously highlighted in the network plot and referred to as the B signature.

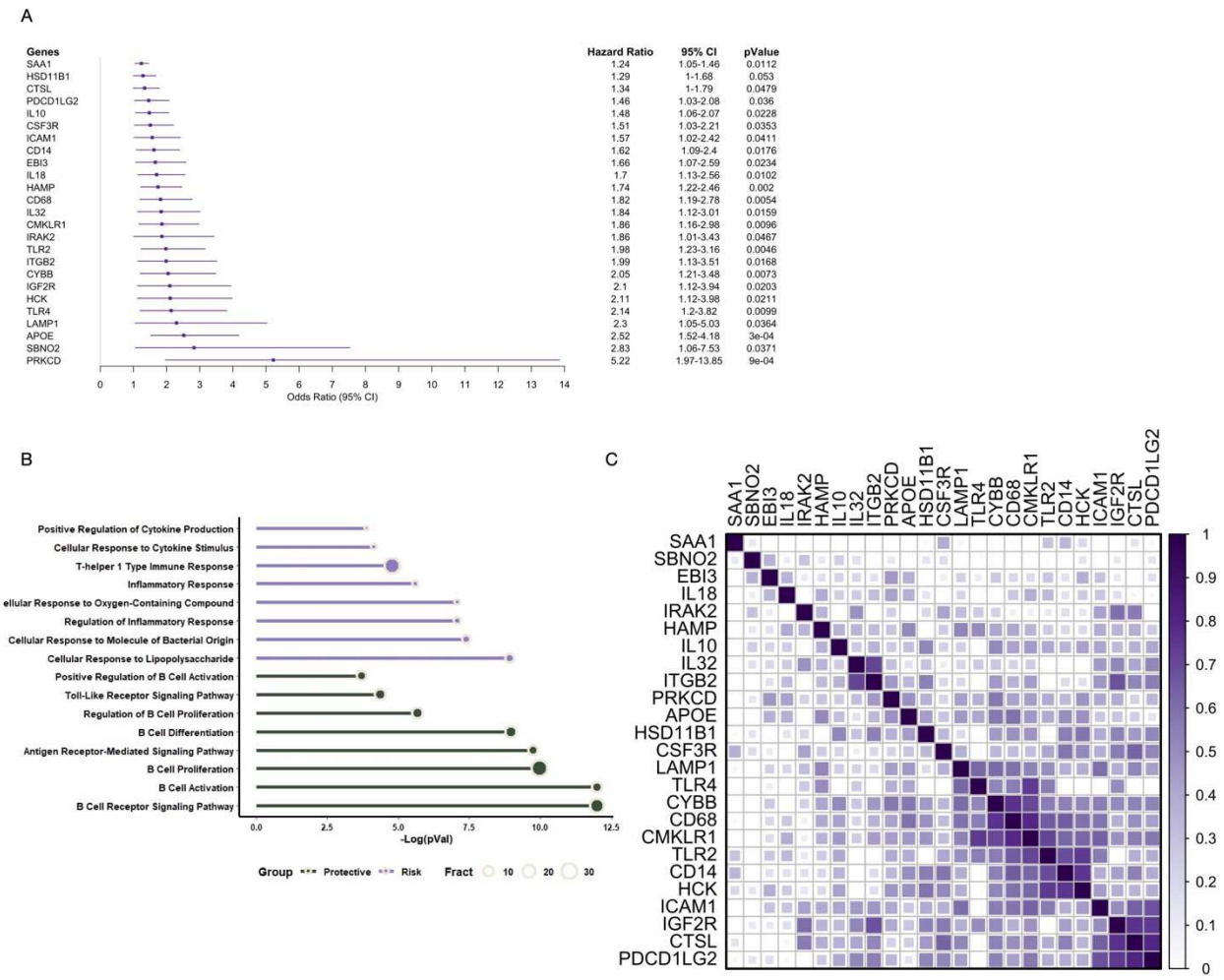

Figure 16. A) Forest plot showing the results of Cox regression analysis for genes significantly associated with progression-free survival (PFS) and associated with adverse outcome. B) GO analysis both protective and risk genes. C) Correlation matrix including protective genes expression values. Correlation coefficients are shown using a green color gradient. Only statistically significant correlations are displayed ($p \leq 0.05$).

This gene signature was subsequently employed to perform unsupervised clustering of the 155 patients included in the training cohort. Notably, expression patterns of the B-cell–related genes stratified the cohort into three distinct groups, defined as High B-cell (HBC), Medium B-cell (MBC), and Low B-cell (LBC), according to increasing levels of signature expression (Figure 17A). Consistent with this classification, the three clusters exhibited a progressive and graded enrichment of non-malignant B-cell gene expression (Figure 17B–C).

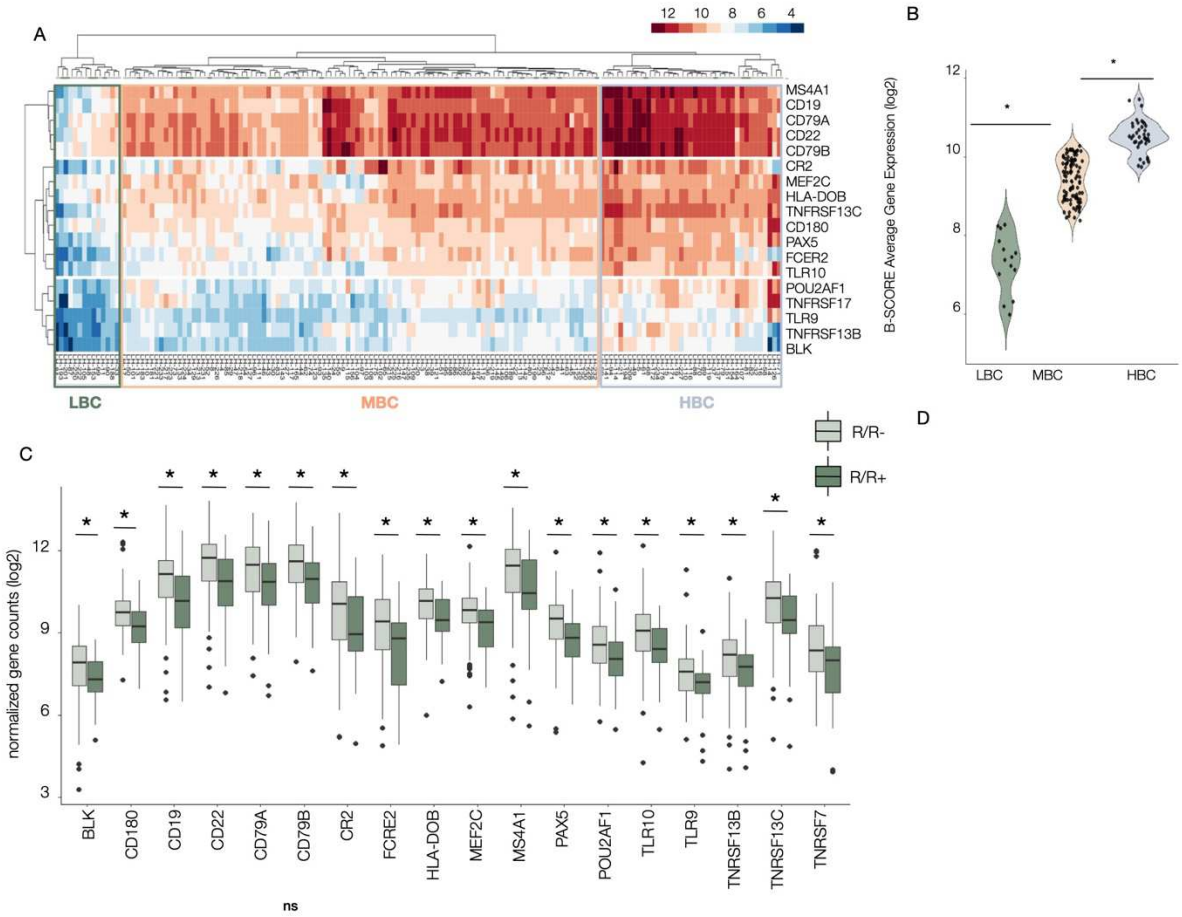

Figure 17. A) Unsupervised clustering including the 18 genes previously highlighted in the network plot and referred to as the B signature. B) Violin plot showing, for each patient, the mean expression value of B signature genes across the three patients groups identified by the unsupervised clustering. C) Boxplot of the 18 genes in R/R− and R/R+ cHLs of the training cohort.

Consistent with these findings, the estimated abundance of naïve B cells progressively increased across the clusters, from the High B-cell (HBC) to the Low B-cell (LBC) group (Figure 18A). Conversely, the predicted abundance of HRS cells showed a decreasing trend from HBC to LBC, in agreement with the model derived from spatial transcriptomic analyses, although this trend did not reach statistical significance (Figure 18B). To further substantiate the inverse relationship between non-malignant B cells and HRS cells, we assessed their association within the training cohort using two independent approaches. Both the B-cell gene signature (Figure 18C) and the estimated abundance of non-tumoral B cells demonstrated a significant inverse correlation with the predicted HRS cell abundance (Figure 18D), thereby providing additional support for our proposed model.

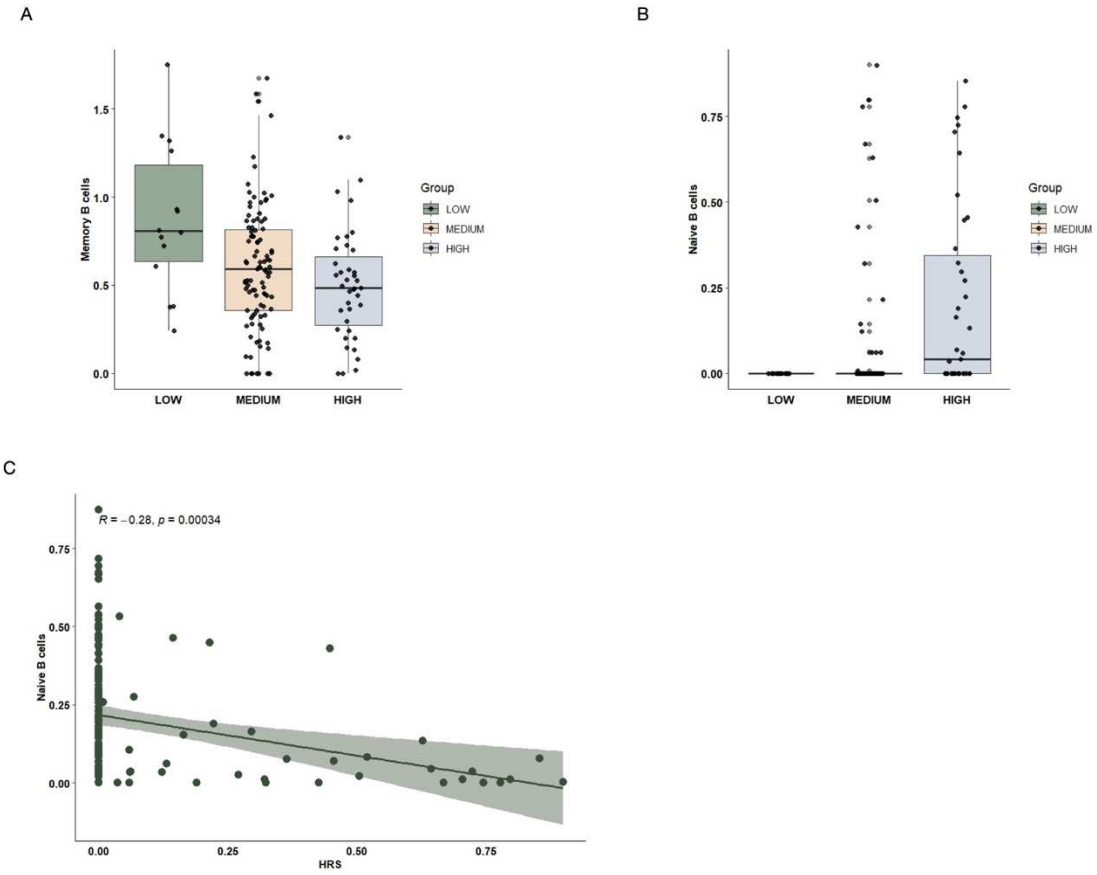

Figure 18. A–B) Boxplot representing the estimated abundance of memory (A) and naïve (B) B cells obtained by deconvolution analysis across the three patients groups identified by the unsupervised clustering. p-value was calculated by Kruskal–Wallis test and considered significant at $p \leq 0.05$. C) Correlation plot between the estimated abundance of naïve B cells and the estimated amount of HRS derived from deconvolution analysis. The p-value was derived from Pearson's correlation analysis.

To evaluate the impact of non-malignant B-cell persistence on clinical aggressiveness, survival analyses were conducted to determine whether the three molecular clusters differed in clinical outcome. Stratification based on B-cell gene expression was significantly associated with progression-free survival (PFS). Patients in the High B-cell (HBC) cluster exhibited the most favorable prognosis, whereas those classified as Low B-cell (LBC) showed a significantly shorter PFS compared with both the HBC and Medium B-cell (MBC) groups (Figure 19A). Consistently, correlation analyses with key clinical variables indicated that the HBC cluster was significantly associated with early-stage disease (I–II), lower incidence of bulky and localized disease, reduced LDH/ULN values, and higher serum albumin levels. In parallel, radiomic parameters—including total metabolic tumor volume (TMTV) and DMAX—were differentially distributed across the three clusters, with higher values observed in the clinically

more aggressive LBC group, in line with their established prognostic significance (Figure 19B–C).

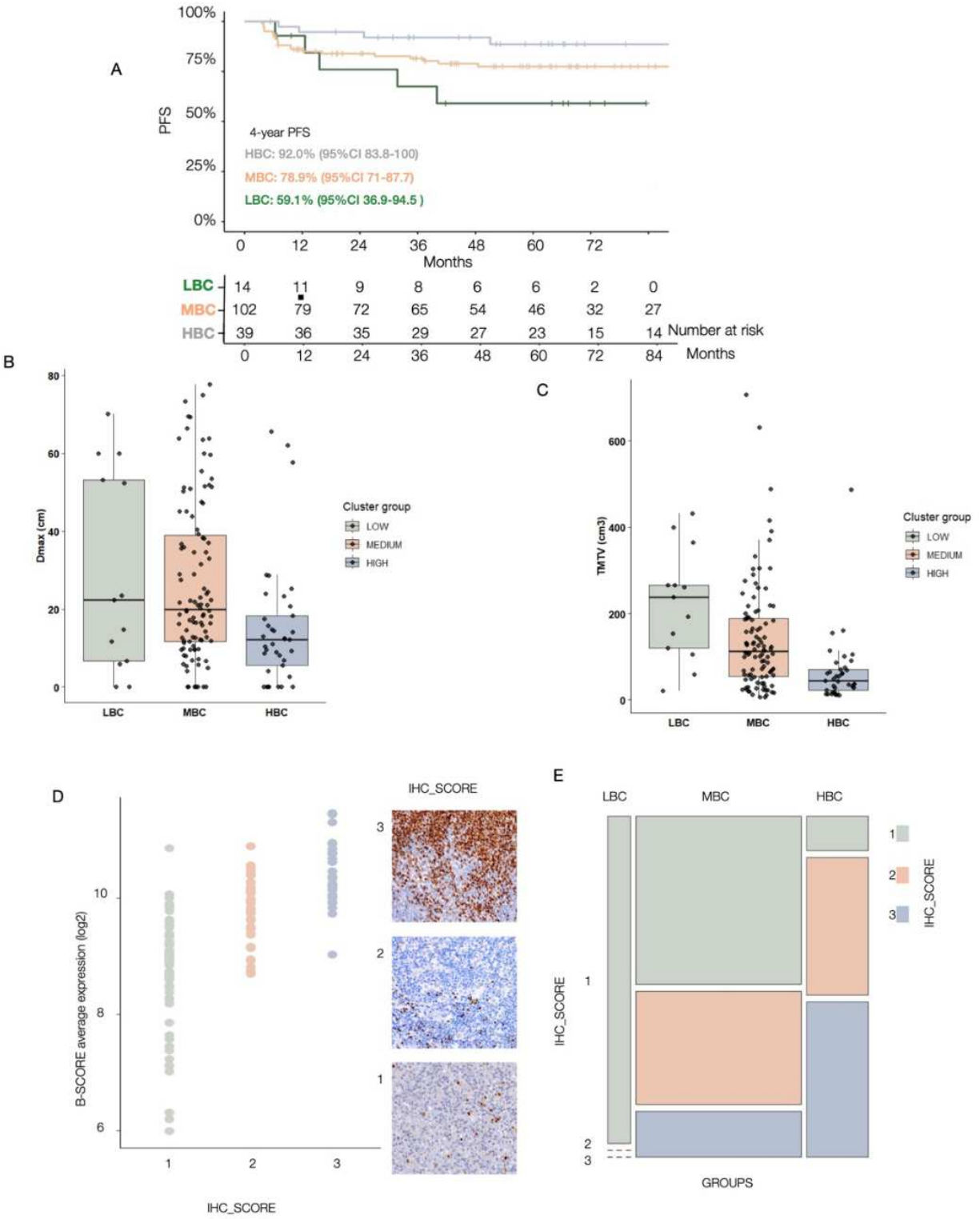

Figure 19. A) Kaplan–Meier curves showing progression-free survival (PFS) of the three patients groups identified by the unsupervised clustering. p-value was calculated by log-rank test and hazard ratio by Cox regression analysis. B–C) Boxplot showing the distribution of radiomic features in the three cluster of patients identified. B) TMTV, C) DMAX. D) Representative IHC images of non-tumoral B cell quantification in cHL biopsies from training cohort, and representation of mean expression values of B cell signature genes across patient groups stratified by IHC score. E) Mosaic plot showing the correlation between patient groups identified by IHC score and those derived from unsupervised clustering based on B cell signature genes.

B-Cell Gene Signature as a Predictor of Clinical Progression in cHL

Although our findings suggested a potential prognostic relevance of the non-malignant B-cell gene signature, we sought to verify whether transcriptomic estimates reliably reflected the actual presence of normal B cells within the tumor microenvironment. To this end, the abundance of non-tumoral B cells was independently assessed by CD20 immunohistochemistry (IHC). IHC-based quantification closely mirrored gene expression data, confirming that the B-cell gene signature faithfully captures the true density of normal B cells within cHL lesions (Figure 19 D–E) and supporting its biological robustness.

On the basis of this validation, we developed a B-cell–specific prognostic score using a penalized regression model applied to the 18-gene signature in the training cohort. Nine genes were retained and integrated into a composite score capable of predicting progression-free survival (PFS), achieving an AUC of 0.73 (95% CI, 0.62–0.84), indicating a good discriminative capacity in identifying patients at risk of progression.

In univariate Cox regression analysis (Table II), several established clinical variables were significantly associated with inferior PFS, including leukocytosis (>15×10^3/mm³; $p = 0.047$), elevated ESR (>50; $p = 0.006$), advanced stage (III–IV; $p < 0.001$), extranodal involvement ($p = 0.047$), and increased Dmax (>20 cm; $p = 0.043$). Notably, the B-cell score demonstrated a strong protective association with outcome (HR 0.26, 95% CI 0.14–0.49; $p < 0.001$), showing a magnitude of effect comparable to, or greater than, that observed for traditional high-risk clinical features. Importantly, in multivariate analysis adjusting for clinically relevant variables, advanced stage (HR 4.20; $p = 0.023$) and the B-cell score (HR 0.37; 95% CI 0.15–0.92; $p = 0.033$) both retained independent prognostic significance. The persistence of statistical significance for the B-cell score after adjustment for established clinical and radiomic factors underscores its robustness and highlights its ability to capture a biologically meaningful component of disease aggressiveness that is not fully reflected by conventional risk parameters.

Notably, while advanced stage remains a cornerstone of clinical risk assessment, the B-cell score emerged as the only microenvironment-derived biomarker independently associated with progression-free survival. This finding suggests that integrating tumor microenvironment biology into prognostic evaluation may provide additional stratification power beyond traditional staging systems.

Table II: Association of clinical variables, radiomic variables and B cells score with PFS in the training cohort.

Clinical Variable	Hazard Ratio (95% ci)	pValue	Hazard Ratio (95% ci)	pValue
Sex (M)	1.16 (0.57-2.36)	0.675	-	
Age (>45)	0.83 (0.38-1.8)	0.635	-	
Albumin (>4 g/dl)	0.43 (0.17-1.07)	0.068	-	
Hemoglobin (>10.5 g/dl)	0.91 (0.32-2.59)	0.854	-	
Leukocytes (>15*10^3 cells/mm^3)	2.35 (1.01-5.47)	0.047	1.13 (0.43-2.98)	0.797
LDH/ULN (>1)	0.95 (0.43-2.13)	0.908	-	
ESR (>50)	3.36 (1.43-7.9)	0.006	1.57 (0.62-3.98)	0.339
Stage (IIB-III-IV)	6.66 (2.33-19.07)	<0.001	4.20 (1.22-14.52)	0.023
Bulky (yes)	1.83 (0.70-4.78)	0.215	-	
Extranodal (yes)	2.05 (1.01-4.15)	0.047	0.64 (0.27-1.53)	0.315
HASENCLEVER (≥3)	1.47 (0.73-2.99)	0.284	-	
TMTV (>100cm)	2.01 (0.96-4.2)	0.063	-	
Dmax (>20cm)	2.19 (1.03-4.68)	0.043	1.27 (0.51-3.20)	0.608
B cells score	0.26 (0.14-0.49)	<0.001	0.37 (0.15-0.92)	0.033

Protective Effects of Non-Malignant B Cells in Aggressive Classical Hodgkin Lymphoma: Validation Analysis

Collectively, these results support a model in which the maintenance of a dense population of non-malignant B cells within the tumor microenvironment represents a clinically meaningful protective factor in classical Hodgkin lymphoma. We independently validated this model in a large, multicenter cohort of cHL patients (Figure 20A; Table I). Cox proportional hazards analysis confirmed the prognostic relevance of the B-cell gene signature, with 13 of the 18 genes (72%) significantly associated with improved progression-free survival (PFS) in the

validation cohort (Figure 20B). Consistently, expression levels of these genes were significantly higher in R/R− compared with R/R+ patients (Figure 20C). In line with findings from the training cohort, unsupervised clustering based on the B-cell signature stratified patients into three distinct groups—Low B-cell (LBC), Medium B-cell (MBC), and High B-cell (HBC)—characterized by markedly different clinical outcomes. Patients in the HBC cluster exhibited significantly superior PFS compared with both MBC and LBC groups, whereas the LBC cluster was associated with the poorest prognosis (Figure 21A). This stratification reflected a progressive and significant increase in B-cell gene expression from LBC to HBC (Figure 21B), occurring independently of CD30 expression levels (Figure 21C). Moreover, an inverse relationship between the estimated abundance of HRS cells and naïve B cells was consistently observed (Figure 21D). Application of the B-score to the validation cohort further confirmed the robustness of this prognostic model, yielding an area under the curve (AUC) of 0.66 (95% CI, 0.52–0.80). Importantly, multivariate analyses incorporating established clinical and radiomic prognostic factors demonstrated that the B-score retained independent prognostic significance and remained strongly associated with improved PFS (Table III).

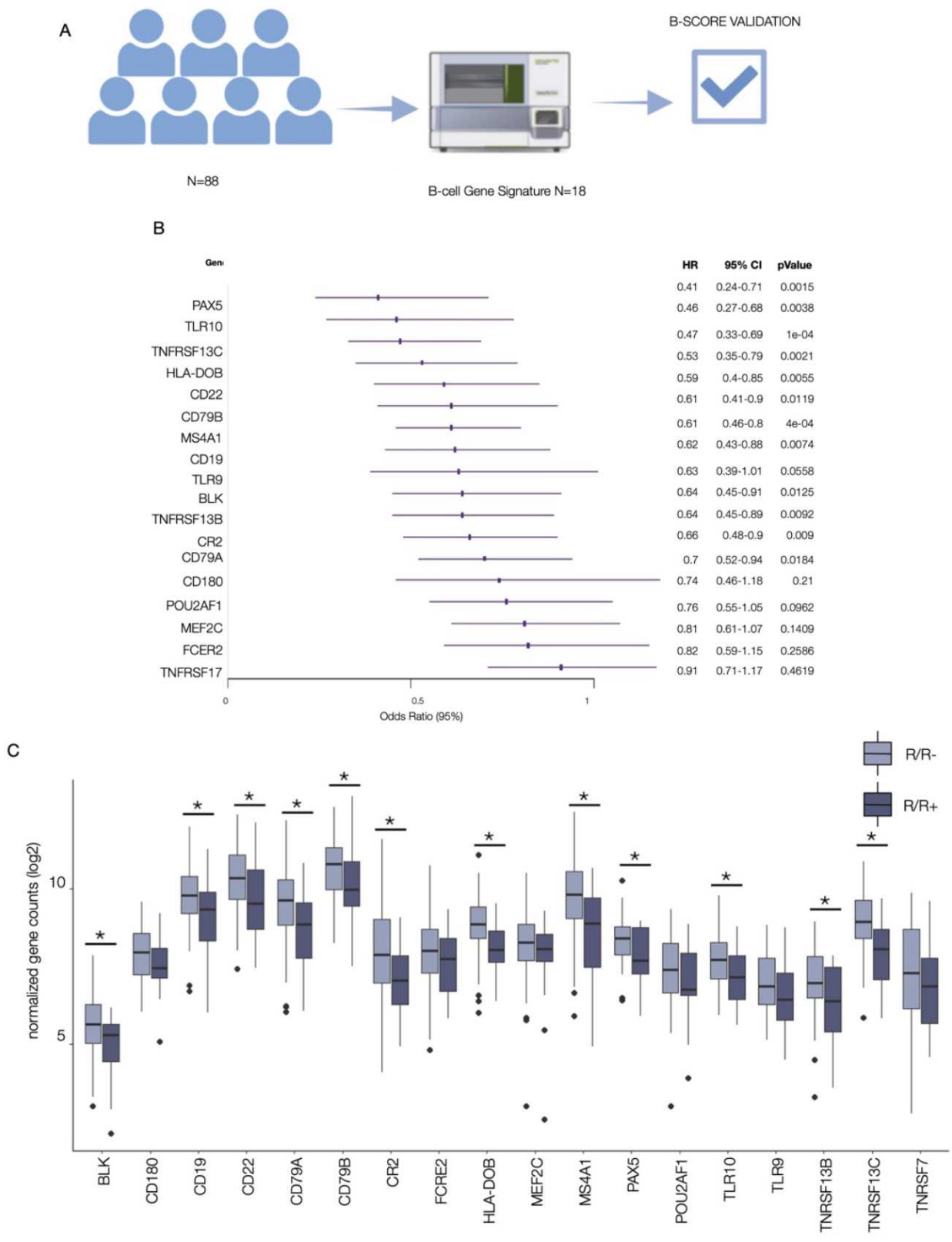

Figure 20. A) Workflow of the digital bar-coding bulk gene-expression profiling in the multicentric retrospective cohort of cHL (validation). B) Forest plot showing the results of Cox regression analysis for the 18 genes of the B cell signature. C) Boxplot showing the expression of B cell signature genes in patients who experienced an event versus those who did not. Statistical significance was assessed using the Wilcoxon test. Comparisons were considered significant at $p \leq 0.05$.

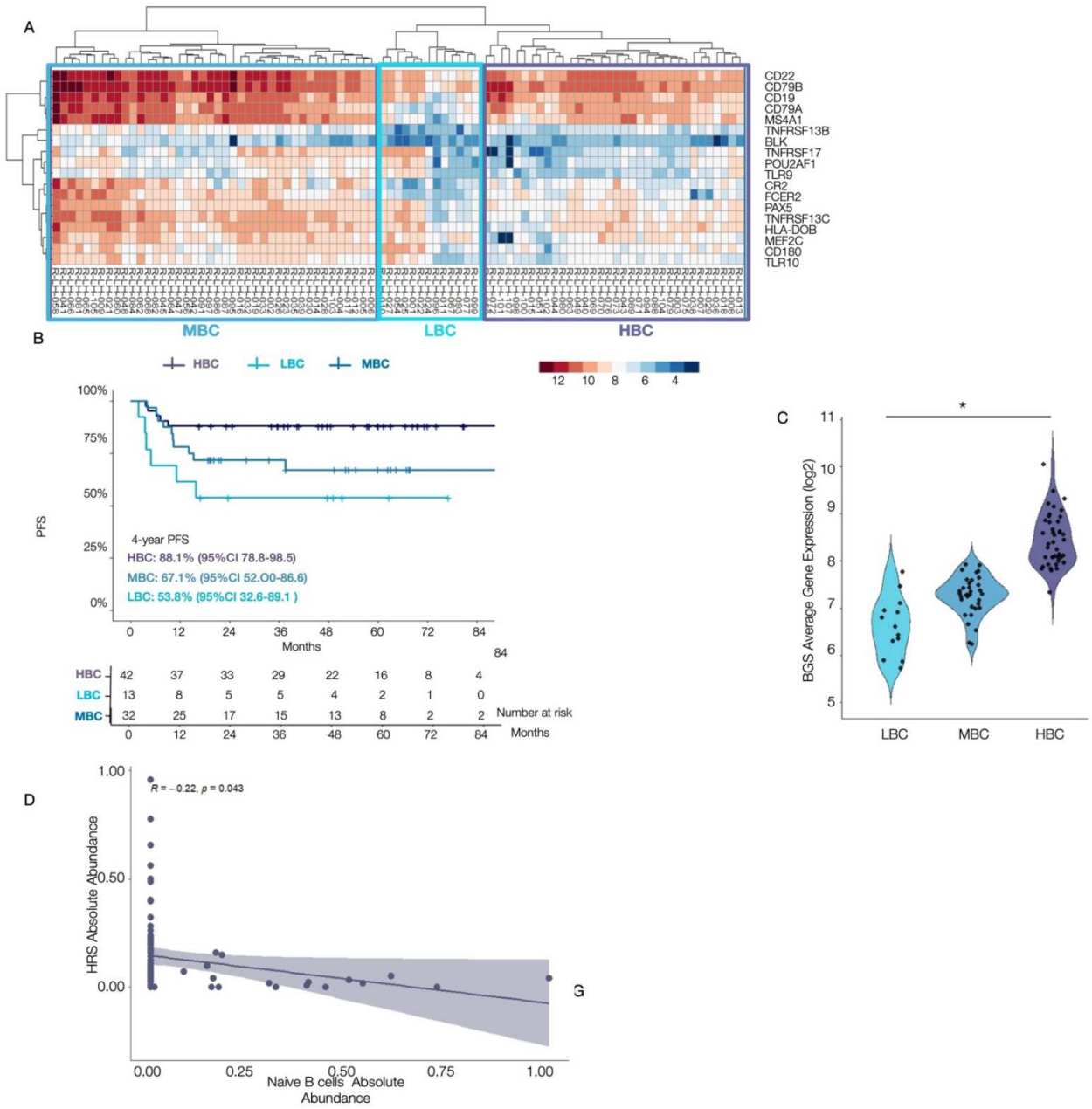

Figure 21. A) Unsupervised clustering based on the expression values of the B signature genes in the validation cohort. B) Kaplan–Meier curves showing progression-free survival (PFS) of the three patients groups identified by the unsupervised clustering in the validation cohort. p-value was calculated by log-rank test and hazard ratio by Cox regression model. C) Violin plot showing, for each patient, the mean expression value of B signature genes across the three patients groups identified by the unsupervised clustering in the validation cohort. D) Correlation plot between the estimated proportions of naïve B cells and HRS cells derived from deconvolution analysis. The p-value was derived from Pearson's correlation analysis.

Table III: Association of clinical variables and B cells score with PFS in the validation cohort.

Clinical Variable	Hazard Ratio (95% ci)	pValue	Hazard Ratio (95% ci)	pValue
Sex (M)	0.49 (0.21-1.16)	0.106	-	
Age (>45)	0.90 (0.30-2.68)	0.850	-	
Albumin (>4 g/dl)	0.40 (0.13-0.22)	0.106	-	
Hemoglobin (>10.5 g/dl)	0.51 (0.20-1.31)	0.163	-	
Leukocytes (>15*10^3 cells/mm^3)	2.18 (0.80-5.99)	0.129	-	
LDH/ULN (>1)	1.01 (0.41-2.51)	0.976	-	
ESR (>50)	1.31 (0.52-3.30)	0.570	-	
Stage (IIB-III-IV)	3.66 (1.08-12.43)	0.038	4.07 (0.91-18.13)	0.065
Bulky (yes)	3.95 (1.37-11.42)	0.011	2.35 (0.76-7.19)	0.136
Extranodal (yes)	0.63 (0.27-1.48)	0.286	-	
HASENCLEVER (≥3)	1.84 (0.71-4.76)	0.211	-	
B cells score	0.25 (0.08-0.80)	0.019	0.18 (0.04-0.80)	0.025

Discussion

This work provides a substantial advance in the understanding of classical Hodgkin lymphoma pathobiology and introduces a novel, biologically grounded prognostic framework for patient stratification. A key innovative aspect of this study lies in the transition from a purely descriptive functional characterization of the tumor microenvironment to the identification of its concrete prognostic clinical implications. By integrating spatially resolved transcriptomics with digital barcoding gene-expression profiling across two large and independent cHL cohorts, we move beyond mapping the cellular and transcriptional architecture of the microenvironment and demonstrate how specific immune components, particularly the non-malignant B-cell compartment, directly influence clinical outcome. Through this integrative approach, we delineate a model in which clinical aggressiveness is dictated by a finely regulated interplay between malignant HRS cells and the surrounding non-malignant B-cell compartment. Our findings indicate that the persistence of non-tumoral B cells within the tumor microenvironment acts not only as a functional modulator of immune dynamics but also as a critical determinant of prognosis, constraining HRS cell expansion and disease progression.

Importantly, the presence of non-malignant B cells is tightly linked to both the composition and functional state of the immune infiltrate, fostering an immune-active microenvironment that counteracts immunosuppression and limits the transcriptional reprogramming of HRS cells. In this context, maintenance of the normal B-cell compartment appears to delay the progressive loss of B-cell identity that characterizes aggressive disease. Together, these results position non-tumoral B cells as key modulators of cHL biology and highlight their potential exploitation as prognostic biomarkers and therapeutic leverage points in classical Hodgkin lymphoma (Figure 22).

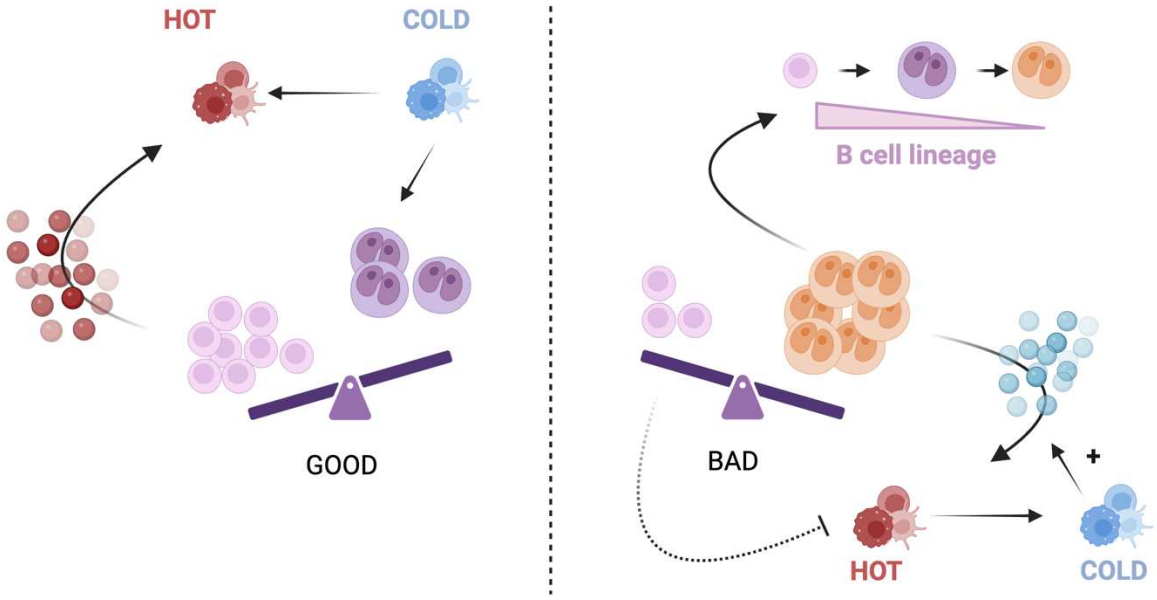

Figure 22 Schematic representation of the non-tumoral/HRS interplay during clinical progression of cHL

This study represents one of the first high-resolution and clinically oriented molecular characterizations of Hodgkin and Reed–Sternberg (HRS) cells in relation to disease aggressiveness. Comprehensive profiling of HRS cells is inherently challenging due to their extreme rarity and dispersed spatial organization within the tumor microenvironment, limitations that persist even with state-of-the-art single-cell RNA sequencing approaches [15,103]. By leveraging spatial transcriptomic technologies, we were able to circumvent these constraints, enabling robust and spatially informed transcriptional profiling of HRS cells irrespective of their density or anatomical distribution, including lesions with a low HRS burden.

This approach uncovered substantial heterogeneity within the HRS compartment and demonstrated that HRS transcriptional programs dynamically evolve with disease progression. We observed that increasing clinical aggressiveness in cHL is associated with a progressive loss of B-cell lineage identity in HRS cells, reflected by the downregulation of canonical B-cell markers and key regulatory transcription factors. This de-differentiation process was particularly evident in relapsed or refractory cases and was accompanied by the acquisition of a more pronounced immunosuppressive phenotype, including increased expression of mediators such as CCL17 and IL13.

These findings suggest that, as HRS cells progressively lose their B-cell features, they gain a greater capacity to remodel the tumor microenvironment in a manner that favors immune escape and disease progression. This concept is consistent with observations in solid tumors, where

phenotypic plasticity is coupled to immune-evasive properties [126,127]. Importantly, this biological shift translates into clinically relevant behavior, as the most aggressive lesions were characterized not only by higher tumor burden but also by a marked depletion of the non-malignant B-cell compartment.

A central observation of this study is the identification of an antagonistic balance between malignant HRS cells and normal B cells within the tumor microenvironment. While increased HRS content has long been associated with adverse prognosis, our data indicate that the reduction of the non-tumoral B-cell population represents an even stronger determinant of clinical aggressiveness.

Although the underlying mechanisms require further investigation, the preservation of the normal B-cell compartment appears to sustain a more immune-active microenvironment and to restrain the expansion and immunosuppressive reprogramming of HRS cells. In this perspective, non-malignant B cells emerge not as passive bystanders, but as clinically relevant modulators of disease behavior [18].

Collectively, these findings support a model in which the clinical course of cHL is influenced by the dynamic equilibrium between tumor cells and the surrounding B-cell compartment, highlighting the potential relevance of this balance for patient risk stratification [128,129,130].

Development of a Novel Prognostic Tool

Building on the biological framework established in this study, we translated the identification of a protective non-malignant B-cell compartment into a clinically applicable prognostic instrument. We developed and validated a B-cell–specific, gene-expression–based score capable of predicting progression-free survival and stratifying patients according to their risk of relapse or refractory disease.

Importantly, this model was derived from and validated in cohorts of patients uniformly treated with standard ABVD-based regimens and including all disease stages at diagnosis. This methodological consistency enhances the clinical interpretability of the results and supports the applicability of the score across the full spectrum of newly diagnosed classical Hodgkin lymphoma. In multivariate analyses adjusted for established clinical and radiomic predictors,

the B-score retained independent prognostic significance, demonstrating that it captures biologically relevant information not encompassed by conventional risk factors.

From a clinical perspective, this tool may support more individualized patient management. The ability to identify, at diagnosis, patients with a biologically defined higher risk of progression may contribute to a more informed therapeutic strategy within standard treatment frameworks. Conversely, recognition of a favorable biological profile may help refine risk-adapted approaches in selected patients.

The strong concordance between the gene-expression–derived score and CD20 immunohistochemical quantification further confirms its biological validity and reinforces its translational potential. Compared with conventional IHC-based assessment, the transcriptomic approach provides greater standardization, reduced operator dependence, and fully quantitative measurement, facilitating integration into multiparametric prognostic algorithms in routine clinical practice.

Clinical Implications and Future Directions

Building on the biological insights generated by this study, we translated the functional characterization of the tumor microenvironment into a clinically actionable prognostic tool. A central strength of this work lies precisely in this transition—from a descriptive molecular dissection of immune components to the development of a quantitative model capable of informing patient risk stratification. By designing and independently validating a B-cell–focused, gene-expression–based prognostic score, we demonstrate that microenvironmental features are not merely biologically relevant but carry direct and independent prognostic significance.

Importantly, the B-cell score retained its prognostic value across both training and validation cohorts, even after adjustment for established clinical and radiomic variables. This indicates that the model captures biologically meaningful information that complements, rather than duplicates, current prognostic frameworks. The integration of this score into existing risk stratification systems may therefore allow a more refined identification of high-risk patients, including those presenting with apparently favorable early-stage disease, who might otherwise be undertreated based on conventional criteria alone.

Beyond its immediate prognostic implications, this model may acquire even greater relevance in the context of the evolving therapeutic landscape of classical Hodgkin lymphoma. The incorporation of novel agents such as anti-CD30 antibody–drug conjugates and immune checkpoint inhibitors into frontline regimens has significantly reshaped treatment paradigms, including in elderly or unfit patients. In this rapidly changing scenario, biologically informed risk stratification tools become essential to guide treatment personalization—both in terms of therapeutic intensification for high-risk individuals and potential de-escalation strategies in biologically favorable cases.

Notably, this study was conceived prior to the widespread adoption of brentuximab vedotin–containing regimens and checkpoint inhibitors in first-line therapy. Future investigations should therefore assess whether the B-cell score retains its predictive and prognostic performance within these modern treatment settings and whether it may help identify patients more likely to benefit from immune-based therapeutic strategies.

The strong concordance observed between the gene-expression–derived score and immunohistochemical quantification of non-malignant B cells further supports the biological robustness of the model. Compared with IHC-based evaluation, the transcriptomic approach offers clear methodological advantages, including improved reproducibility, reduced operator-dependent variability, and fully quantitative output. These characteristics make the B-cell score particularly well suited for incorporation into multiparametric prognostic algorithms and for integration into future precision medicine strategies in classical Hodgkin lymphoma.

Conclusion

This study provides a comprehensive molecular and spatial characterization of HRS cells and their interactions within the cHL tumor microenvironment, revealing mechanisms that drive immune escape and disease progression. Crucially, we demonstrate a protective role for non-malignant B cells, whose presence mitigates tumor aggressiveness and offers a potential avenue for patient risk stratification. By integrating deep transcriptomic profiling with spatial and morphological analyses, we achieve a multidimensional understanding of the cHL ecosystem, highlighting how both cellular heterogeneity and the organization of cell populations shape the biology of the tumor. Collectively, these findings advance our understanding of cHL pathogenesis and establish a foundation for the development of more precise prognostic tools and targeted therapeutic strategies.

Bibliography

1. Pauline Brice, Eric de Kerviler, Jonathan W Friedberg. Classical Hodgkin lymphoma. *The Lancet* **398**, 1518–1527 (2021).
2. National Cancer Institute Surveillance Epidemiology and End Results Program. *SEER Cancer Stat Facts: Hodgkin Lymphoma*. https://seer.cancer.gov/statfacts/html/hodg.html.
3. Huang, J. *et al.* Incidence, mortality, risk factors, and trends for Hodgkin lymphoma: a global data analysis. *J Hematol Oncol* **15**, 57 (2022).
4. Lynny Yung and David Linch. Hodgkin's lymphoma. *Lancet* **361**, 943–951 (2003).
5. Linghui Zhou, Yujiao Deng, Na Li, Yi Zheng, Tian Tian, Zhen Zhai, Si Yang, Qian Hao, Ying Wu, Dingli Song, Dai Zhang, Jun Lyu & Zhijun Dai. Global, regional, and national burden of Hodgkin lymphoma from 1990 to 2017: estimates from the 2017 Global Burden of Disease study. *Journal of Hematology & Oncology* **12**, (2019).
6. Mangone, L. *et al.* Incidence, mortality, and survival of hematological malignancies in Northern Italian patients: an update to 2020. *Front. Oncol.* **13**, 1182971 (2023).
7. Swerdlow SH, Campo E, Harris NL, Jaffe ES, Pileri SA, Stein H, Thiele J. *WHO Classification of Tumours of Haematopoietic and Lymphoid Tissues WHO Classification of Tumours*. vol. 2 (2017).
8. Allemani, C. *et al.* Hodgkin disease survival in Europe and the U.S.: Prognostic significance of morphologic groups. *Cancer* **107**, 352–360 (2006).
9. Biggar, R. J. *et al.* Hodgkin lymphoma and immunodeficiency in persons with HIV/AIDS. *Blood* **108**, 3786–3791 (2006).
10. 10. Shimabukuro-Vornhagen, A. *et al.* Lymphocyte-Rich Classical Hodgkin's Lymphoma: Clinical Presentation and Treatment Outcome in 100 Patients Treated Within German Hodgkin's Study Group Trials. *JCO* **23**, 5739–5745 (2005).
11. Klimm, B. *et al.* Lymphocyte-Depleted Classical Hodgkin's Lymphoma: A Comprehensive Analysis From the German Hodgkin Study Group. *JCO* **29**, 3914–3920 (2011).
12. Joseph M. Connors, Wendy Cozen, Christian Steidl, Antonino Carbone, Richard T. Hoppe, Hans-Henning Flechtner & Nancy L. Bartlett. Hodgkin lymphoma. *Nature Reviews Disease Primers* **6**, (2020).

13. Küppers, R. *et al.* Hodgkin disease: Hodgkin and Reed-Sternberg cells picked from histological sections show clonal immunoglobulin gene rearrangements and appear to be derived from B cells at various stages of development. *Proc. Natl. Acad. Sci. U.S.A.* **91**, 10962–10966 (1994).
14. Kanzler, H., Küppers, R., Hansmann, M. L. & Rajewsky, K. Hodgkin and Reed-Sternberg cells in Hodgkin's disease represent the outgrowth of a dominant tumor clone derived from (crippled) germinal center B cells. *The Journal of experimental medicine* **184**, 1495–1505 (1996).
15. Schwering, I. *et al.* Loss of the B-lineage–specific gene expression program in Hodgkin and Reed-Sternberg cells of Hodgkin lymphoma. *Blood* **101**, 1505–1512 (2003).
16. Hertel, C. B., Zhou, X., Hamilton-Dutoit, S. J. & Junker, S. Loss of B cell identity correlates with loss of B cell-specific transcription factors in Hodgkin/Reed-Sternberg cells of classical Hodgkin lymphoma. *Oncogene* **21**, 4908–4920 (2002).
17. Venkataraman, G. *et al.* Aberrant T-cell antigen expression in classical Hodgkin lymphoma is associated with decreased event-free survival and overall survival. *Blood* **121**, 1795–1804 (2013).
18. Weniger, M. A. & Küppers, R. Molecular biology of Hodgkin lymphoma. *Leukemia* **35**, 968–981 (2021).
19. Steidl, C., Connors, J. M. & Gascoyne, R. D. Molecular Pathogenesis of Hodgkin's Lymphoma: Increasing Evidence of the Importance of the Microenvironment. *JCO* **29**, 1812–1826 (2011).
20. Vockerodt, M. *et al.* The Epstein–Barr virus and the pathogenesis of lymphoma. *The Journal of Pathology* **235**, 312–322 (2015).
21. G. Pallesen, S.J. Hamilton-Dutoit, M. Rowe, L.S. Young. Expression of Epstein-Barr virus latent gene products in tumour cells of Hodgkin's disease. *The Lancet* **337**, 320–322 (1991).
22. Tiacci, E. *et al.* Pervasive mutations of JAK-STAT pathway genes in classical Hodgkin lymphoma. *Blood* **131**, 2454–2465 (2018).
23. Weniger, M. A. *et al.* Mutations of the tumor suppressor gene SOCS-1 in classical Hodgkin lymphoma are frequent and associated with nuclear phospho-STAT5 accumulation. *Oncogene* **25**, 2679–2684 (2006).
24. Lollies, A. *et al.* An oncogenic axis of STAT-mediated BATF3 upregulation causing MYC activity in classical Hodgkin lymphoma and anaplastic large cell lymphoma. *Leukemia* **32**, 92–101 (2018).

25. Mathas, S. Aberrantly expressed c-Jun and JunB are a hallmark of Hodgkin lymphoma cells, stimulate proliferation and synergize with NF-kappaB. *The EMBO Journal* **21**, 4104– 4113 (2002).
26. Dutton, A., Reynolds, G. M., Dawson, C. W., Young, L. S. & Murray, P. G. Constitutive activation of phosphatidyl-inositide 3 kinase contributes to the survival of Hodgkin's lymphoma cells through a mechanism involving Akt kinase and mTOR. *J. Pathol.* **205**, 498–506 (2005).
27. Georgakis, G. V. *et al.* Inhibition of the phosphatidylinositol-3 kinase/Akt promotes G1 cell cycle arrest and apoptosis in Hodgkin lymphoma. *Br J Haematol* **132**, 503–511 (2006).
28. Renné, C., Willenbrock, K., Küppers, R., Hansmann, M.-L. & Bräuninger, A. Autocrine- and paracrine-activated receptor tyrosine kinases in classic Hodgkin lymphoma. *Blood* **105**, 4051–4059 (2005).
29. Lamprecht, B. *et al.* Derepression of an endogenous long terminal repeat activates the CSF1R proto-oncogene in human lymphoma. *Nat Med* **16**, 571–579 (2010).
30. Jundt, F. *et al.* Aberrant expression of Notch1 interferes with the B-lymphoid phenotype of neoplastic B cells in classical Hodgkin lymphoma. *Leukemia* **22**, 1587–1594 (2008).
31. Küppers, R. Advances in Hodgkin lymphoma research. *Trends in Molecular Medicine* S1471491424002715 (2024) doi:10.1016/j.molmed.2024.10.004.
32. Green, M. R. *et al.* Integrative analysis reveals selective 9p24.1 amplification, increased PD-1 ligand expression, and further induction via JAK2 in nodular sclerosing Hodgkin lymphoma and primary mediastinal large B-cell lymphoma. *Blood* **116**, 3268–3277 (2010).
33. Roemer, M. G. M. *et al. PD-L1* and *PD-L2* Genetic Alterations Define Classical Hodgkin Lymphoma and Predict Outcome. *JCO* **34**, 2690–2697 (2016).
34. Younes, A. & Ansell, S. M. Novel agents in the treatment of Hodgkin lymphoma: Biological basis and clinical results. *Seminars in Hematology* **53**, 186–189 (2016).
35. Roemer, M. G. M. *et al.* Classical Hodgkin Lymphoma with Reduced β2M/MHC Class I Expression Is Associated with Inferior Outcome Independent of 9p24.1 Status. *Cancer Immunology Research* **4**, 910–916 (2016).
36. Steidl, C. *et al.* MHC class II transactivator CIITA is a recurrent gene fusion partner in lymphoid cancers. *Nature* **471**, 377–381 (2011).

37. Abdul Razak, F. R., Diepstra, A., Visser, L. & Van Den Berg, A. CD58 mutations are common in Hodgkin lymphoma cell lines and loss of CD58 expression in tumor cells occurs in Hodgkin lymphoma patients who relapse. *Genes Immun* **17**, 363–366 (2016).
38. Aldinucci, D., Gloghini, A., Pinto, A., De Filippi, R. & Carbone, A. The classical Hodgkin's lymphoma microenvironment and its role in promoting tumour growth and immune escape. *The Journal of Pathology* **221**, 248–263 (2010).
39. Steidl, C. *et al.* Tumor-Associated Macrophages and Survival in Classic Hodgkin's Lymphoma. *N Engl J Med* **362**, 875–885 (2010).
40. Carey, C. D. *et al.* Topological analysis reveals a PD-L1-associated microenvironmental niche for Reed-Sternberg cells in Hodgkin lymphoma. *Blood* **130**, 2420–2430 (2017).
41. Pinto, A. *et al.* Human eosinophils express functional CD30 ligand and stimulate proliferation of a Hodgkin's disease cell line. *Blood* **88**, 3299–3305 (1996).
42. Aoki, T. *et al.* Single-Cell Transcriptome Analysis Reveals Disease-Defining T-cell Subsets in the Tumor Microenvironment of Classic Hodgkin Lymphoma. *Cancer Discovery* **10**, 406–421 (2020).
43. Steidl, C. *et al.* CSF1R Expression of Hodgkin Reed Sternberg Cells Is Associated with the Number of Macrophages in the Tumor Microenvironment and Is Correlated with Treatment Outcome. *Blood* **118**, 427–427 (2011).
44. Mariuzza, R. A., Shahid, S. & Karade, S. S. The immune checkpoint receptor LAG3: Structure, function, and target for cancer immunotherapy. *Journal of Biological Chemistry* **300**, 107241 (2024).
45. Wein, F. & Küppers, R. The role of T cells in the microenvironment of Hodgkin lymphoma. *Journal of Leukocyte Biology* **99**, 45–50 (2016).
46. Cattaruzza, L. *et al.* Functional coexpression of Interleukin (IL)-7 and its receptor (IL-7R) on Hodgkin and Reed-Sternberg cells: Involvement of IL-7 in tumor cell growth and microenvironmental interactions of Hodgkin's lymphoma. *Intl Journal of Cancer* **125**, 1092–1101 (2009).
47. Ullrich, K. *et al.* The IL-15 cytokine system provides growth and survival signals in Hodgkin lymphoma and enhances the inflammatory phenotype of HRS cells. *Leukemia* **29**, 1213–1218 (2015).
48. Cheson, B. D. *et al.* Recommendations for Initial Evaluation, Staging, and Response Assessment of Hodgkin and Non-Hodgkin Lymphoma: The Lugano Classification. *JCO* **32**, 3059–3067 (2014).

49. Eichenauer, D. A. *et al.* Hodgkin lymphoma: ESMO Clinical Practice Guidelines for diagnosis, treatment and follow-up. *Annals of Oncology* **29**, iv19–iv29 (2018).
50. Hasenclever, D. *et al.* A Prognostic Score for Advanced Hodgkin's Disease. *N Engl J Med* **339**, 1506–1514 (1998).
51. Moccia, A. A. *et al.* International Prognostic Score in Advanced-Stage Hodgkin's Lymphoma: Altered Utility in the Modern Era. *JCO* **30**, 3383–3388 (2012).
52. Rodday, A. M. *et al.* The Advanced-Stage Hodgkin Lymphoma International Prognostic Index: Development and Validation of a Clinical Prediction Model From the HoLISTIC Consortium. *JCO* **41**, 2076–2086 (2023).
53. Buccheri, V. *et al.* External validation and calibration of the HOLISTIC Consortium's advanced-stage Hodgkin lymphoma international prognostic index (A- HIPI) in the Brazilian Hodgkin lymphoma registry. *Br J Haematol* bjh.19824 (2024) doi:10.1111/bjh.19824.
54. Meignan, M., Gallamini, A., Meignan, M., Gallamini, A. & Haioun, C. Report on the First International Workshop on interim-PET scan in lymphoma. *Leukemia & Lymphoma* **50**, 1257–1260 (2009).
55. Gallamini, A. *et al.* Early Interim 2-[^{18}F]Fluoro-2-Deoxy-D-Glucose Positron Emission Tomography Is Prognostically Superior to International Prognostic Score in Advanced-Stage Hodgkin's Lymphoma: A Report From a Joint Italian-Danish Study. *JCO* **25**, 3746–3752 (2007).
56. Hutchings, M. *et al.* FDG-PET after two cycles of chemotherapy predicts treatment failure and progression-free survival in Hodgkin lymphoma. *Blood* **107**, 52–59 (2006).
57. Connors, J. M. *et al.* Brentuximab Vedotin with Chemotherapy for Stage III or IV Hodgkin's Lymphoma. *N Engl J Med* **378**, 331–344 (2018).
58. Herrera, A. F. *et al.* Nivolumab+AVD in Advanced-Stage Classic Hodgkin's Lymphoma. *N Engl J Med* **391**, 1379–1389 (2024).
59. Engert, A. *et al.* Reduced Treatment Intensity in Patients with Early-Stage Hodgkin's Lymphoma. *N Engl J Med* **363**, 640–652 (2010).
60. Eich, H. T. *et al.* Intensified Chemotherapy and Dose-Reduced Involved-Field Radiotherapy in Patients With Early Unfavorable Hodgkin's Lymphoma: Final Analysis of the German Hodgkin Study Group HD11 Trial. *JCO* **28**, 4199–4206 (2010).
61. Radford, J. *et al.* Results of a Trial of PET-Directed Therapy for Early-Stage Hodgkin's Lymphoma. *N Engl J Med* **372**, 1598–1607 (2015).

62. André, M. P. E. *et al.* Early Positron Emission Tomography Response–Adapted Treatment in Stage I and II Hodgkin Lymphoma: Final Results of the Randomized EORTC/LYSA/FIL H10 Trial. *JCO* **35**, 1786–1794 (2017).
63. Federico, M. *et al.* Long-Term Follow-Up of the Response-Adapted Intergroup EORTC/LYSA/FIL H10 Trial for Localized Hodgkin Lymphoma. *JCO* **42**, 19–25 (2024).
64. Gillessen, S. *et al.* Intensified treatment of patients with early stage, unfavourable Hodgkin lymphoma: long-term follow-up of a randomised, international phase 3 trial of the German Hodgkin Study Group (GHSG HD14). *The Lancet Haematology* **8**, e278–e288 (2021).
65. Fornecker, L.-M. *et al.* Brentuximab Vedotin Plus AVD for First-Line Treatment of Early-Stage Unfavorable Hodgkin Lymphoma (BREACH): A Multicenter, Open-Label, Randomized, Phase II Trial. *JCO* **41**, 327–335 (2023).
66. Bröckelmann, P. J. *et al.* Nivolumab and Doxorubicin, Vinblastine, and Dacarbazine in Early-Stage Unfavorable Hodgkin Lymphoma: Final Analysis of the Randomized German Hodgkin Study Group Phase II NIVAHL Trial. *JCO* **41**, 1193–1199 (2023).
67. ABVD versus BEACOPP for Hodgkin's Lymphoma. *N Engl J Med* **365**, 1544–1546 (2011).
68. Skoetz, N. *et al.* Effect of initial treatment strategy on survival of patients with advanced-stage Hodgkin's lymphoma: a systematic review and network meta-analysis. *The Lancet Oncology* **14**, 943–952 (2013).
69. Luminari, S. *et al.* Long-Term Follow-Up of the Response-Adjusted Therapy for Advanced Hodgkin Lymphoma Trial. *JCO* **42**, 13–18 (2024).
70. Federico, M. *et al.* High-Dose Therapy and Autologous Stem-Cell Transplantation Versus Conventional Therapy for Patients With Advanced Hodgkin's Lymphoma Responding to Front-Line Therapy. *JCO* **21**, 2320–2325 (2003).
71. Borchmann, P. *et al.* Assessing the efficacy and tolerability of PET-guided BrECADD versus eBEACOPP in advanced-stage, classical Hodgkin lymphoma (HD21): a randomised, multicentre, parallel, open-label, phase 3 trial. *The Lancet* **404**, 341–352 (2024).
72. Allen, P. B. *et al.* Pembrolizumab followed by AVD in untreated early unfavorable and advanced-stage classical Hodgkin lymphoma. *Blood* **137**, 1318–1326 (2021).

73. Herrera, A. F. *et al.* SWOG S1826, a randomized study of nivolumab(N)-AVD versus brentuximab vedotin(BV)-AVD in advanced stage (AS) classic Hodgkin lymphoma (HL). *JCO* **41**, LBA4–LBA4 (2023).
74. Ansell, S. M. Hodgkin lymphoma: 2025 update on diagnosis, risk-stratification, and management. *American J Hematol* **99**, 2367–2378 (2024).
75. Horning, S. J. Primary refractory Hodgkin's disease. *Annals of Oncology* **9**, s97–s101 (1998).
76. Schmitz, N. *et al.* Aggressive conventional chemotherapy compared with high-dose chemotherapy with autologous haemopoietic stem-cell transplantation for relapsed chemosensitive Hodgkin's disease: a randomised trial. *The Lancet* **359**, 2065–2071 (2002).
77. Driessen, J., Tonino, S. H., Moskowitz, A. J. & Kersten, M. J. How to choose first salvage therapy in Hodgkin lymphoma: traditional chemotherapy vs novel agents. *Hematology* **2021**, 240–246 (2021).
78. Moskowitz, A. J. *et al.* Pretransplantation functional imaging predicts outcome following autologous stem cell transplantation for relapsed and refractory Hodgkin lymphoma. *Blood* **116**, 4934–4937 (2010).
79. Shah, G. L. *et al.* Risk factors predicting outcomes for primary refractory hodgkin lymphoma patients treated with salvage chemotherapy and autologous stem cell transplantation. *Br J Haematol* **175**, 440–447 (2016).
80. Martínez, C. *et al.* Identification of prognostic factors predicting outcome in Hodgkin's lymphoma patients relapsing after autologous stem cell transplantation. *Annals of Oncology* **24**, 2430–2434 (2013).
81. Morschhauser, F. *et al.* Risk-Adapted Salvage Treatment With Single or Tandem Autologous Stem-Cell Transplantation for First Relapse/Refractory Hodgkin's Lymphoma: Results of the Prospective Multicenter H96 Trial by the GELA/SFGM Study Group. *JCO* **26**, 5980–5987 (2008).
82. Younes, A. *et al.* Results of a Pivotal Phase II Study of Brentuximab Vedotin for Patients With Relapsed or Refractory Hodgkin's Lymphoma. *JCO* **30**, 2183–2189 (2012).
83. Moskowitz, A. J. *et al.* PET-adapted sequential salvage therapy with brentuximab vedotin followed by augmented ifosamide, carboplatin, and etoposide for patients with relapsed and refractory Hodgkin's lymphoma: a non-randomised, open-label, single-centre, phase 2 study. *The Lancet Oncology* **16**, 284–292 (2015).

84. Marie José Kersten *et al.* Combining brentuximab vedotin with dexamethasone, high-dose cytarabine and cisplatin as salvage treatment in relapsed or refractory Hodgkin lymphoma: the phase II HOVON/LLPC Transplant BRaVE study. *haematol* **106**, 1129–1137 (2020).
85. Moskowitz, C. H. *et al.* Brentuximab vedotin as consolidation therapy after autologous stem-cell transplantation in patients with Hodgkin's lymphoma at risk of relapse or progression (AETHERA): a randomised, double-blind, placebo-controlled, phase 3 trial. *The Lancet* **385**, 1853–1862 (2015).
86. Chen, R. *et al.* Phase II Study of the Efficacy and Safety of Pembrolizumab for Relapsed/Refractory Classic Hodgkin Lymphoma. *JCO* **35**, 2125–2132 (2017).
87. Zinzani, P. L. *et al.* Pembrolizumab monotherapy in patients with primary refractory classical hodgkin lymphoma who relapsed after salvage autologous stem cell transplantation and/or brentuximab vedotin therapy: KEYNOTE-087 subgroup analysis. *Leukemia & Lymphoma* **61**, 950–954 (2020).
88. Carreau, N. A. *et al.* Checkpoint Blockade Treatment May Sensitize Hodgkin Lymphoma to Subsequent Therapy. *The Oncologist* **25**, 878–885 (2020).
89. Merryman, R. W. *et al.* Autologous stem cell transplantation after anti-PD-1 therapy for multiply relapsed or refractory Hodgkin lymphoma. *Blood Advances* **5**, 1648–1659 (2021).
90. Casadei, B. *et al.* Effectiveness of chemotherapy after anti-PD-1 blockade failure for relapsed and refractory Hodgkin lymphoma. *Cancer Medicine* **9**, 7830–7836 (2020).
91. Kuruvilla, J. *et al.* Pembrolizumab versus brentuximab vedotin in relapsed or refractory classical Hodgkin lymphoma (KEYNOTE-204): an interim analysis of a multicentre, randomised, open-label, phase 3 study. *The Lancet Oncology* **22**, 512–524 (2021).
92. Advani, R. H. *et al.* Brentuximab vedotin in combination with nivolumab in relapsed or refractory Hodgkin lymphoma: 3-year study results. *Blood* **138**, 427–438 (2021).
93. 93. Barrington, S. F. & Kluge, R. FDG PET for therapy monitoring in Hodgkin and non- Hodgkin lymphomas. *Eur J Nucl Med Mol Imaging* **44**, 97–110 (2017).
94. Hatt, M. *et al.* 18 F-FDG PET Uptake Characterization Through Texture Analysis: Investigating the Complementary Nature of Heterogeneity and Functional Tumor Volume in a Multi–Cancer Site Patient Cohort. *J Nucl Med* **56**, 38–44 (2015).
95. Mettler, J. *et al.* Metabolic Tumor Volume for Response Prediction in Advanced-Stage Hodgkin Lymphoma. *J Nucl Med* **60**, 207–211 (2019).

96. Moskowitz, A. J. *et al.* Prognostic significance of baseline metabolic tumor volume in relapsed and refractory Hodgkin lymphoma. *Blood* **130**, 2196–2203 (2017).
97. Rossi, C. *et al.* High-risk stage IIB Hodgkin lymphoma treated in the H10 and AHL2011 trials: total metabolic tumor volume is a useful risk factor to stratify patients at baseline. *haematol* **107**, 2897–2904 (2022).
98. Herraez, I. *et al.* Total Lesion Glycolysis Improves Tumor Burden Evaluation and Risk Assessment at Diagnosis in Hodgkin Lymphoma. *JCM* **10**, 4396 (2021).
99. Driessen, J. *et al.* Prognostic model using 18F-FDG PET radiomics predicts progression-free survival in relapsed/refractory Hodgkin lymphoma. *Blood Advances* **7**, 6732–6743 (2023).
100. Cottereau, A.-S. *et al.* 18 F-FDG PET Dissemination Features in Diffuse Large B-Cell Lymphoma Are Predictive of Outcome. *J Nucl Med* **61**, 40–45 (2020).
101. Ceriani, L. & Zucca, E. *D*max : A simple and reliable PET/CT-derived new biomarker of lymphoma outcome? *Hematological Oncology* **40**, 843–845 (2022).
102. Durmo, R. *et al.* Prognostic value of lesion dissemination in doxorubicin, bleomycin, vinblastine, and dacarbazine-treated, interimPET-negative classical Hodgkin Lymphoma patients: A radio-genomic study. *Hematological Oncology* **40**, 645–657 (2022).
103. Tiacci, E. *et al.* Analyzing primary Hodgkin and Reed-Sternberg cells to capture the molecular and cellular pathogenesis of classical Hodgkin lymphoma. *Blood* **120**, 4609–4620 (2012).
104. Opinto, G. *et al.* Hodgkin Lymphoma: A Special Microenvironment. *JCM* **10**, 4665 (2021).
105. Stewart, B. J. *et al.* Spatial and molecular profiling of the mononuclear phagocyte network in Classic Hodgkin lymphoma. *Blood* blood.2022015575 (2023) doi:10.1182/blood.2022015575.
106. Chan, F. C. *et al.* Prognostic Model to Predict Post-Autologous Stem-Cell Transplantation Outcomes in Classical Hodgkin Lymphoma. *JCO* **35**, 3722–3733 (2017).
107. Scott, D. W. *et al.* Gene Expression–Based Model Using Formalin-Fixed Paraffin- Embedded Biopsies Predicts Overall Survival in Advanced-Stage Classical Hodgkin Lymphoma. *JCO* **31**, 692–700 (2013).

108. Steidl, C. *et al.* Gene expression profiling of microdissected Hodgkin Reed-Sternberg cells correlates with treatment outcome in classical Hodgkin lymphoma. *Blood* **120**, 3530– 3540 (2012).

109. Van Den Berg, A., Visser, L. & Poppema, S. High Expression of the CC Chemokine TARC in Reed-Sternberg Cells. *The American Journal of Pathology* **154**, 1685–1691 (1999).

110. Diepstra, A. *et al.* Elevated serum TARC levels precede classic Hodgkin lymphoma diagnosis by several years. *Blood* **142**, 1928–1931 (2023).

111. Plattel, W. J. *et al.* Plasma thymus and activation-regulated chemokine as an early response marker in classical Hodgkin's lymphoma. *Haematologica* **97**, 410–415 (2012).

112. Plattel, W. J. *et al.* Interim thymus and activation regulated chemokine *versus* interim18 F-fluorodeoxyglucose positron-emission tomography in classical Hodgkin lymphoma response evaluation. *Br J Haematol* **190**, 40–44 (2020).

113. Driessen, J. *et al.* Prognostic value of TARC and quantitative PET parameters in relapsed or refractory Hodgkin lymphoma patients treated with brentuximab vedotin and DHAP. *Leukemia* **36**, 2853–2862 (2022).

114. Jachimowicz, R. D. *et al.* Gene expression-based outcome prediction in advanced stage classical Hodgkin lymphoma treated with BEACOPP. *Leukemia* **35**, 3589–3593 (2021).

115. Burton, C. H. *et al.* APPLICATION OF a GENE EXPRESSION-BASED MODEL IN COMBINATION WITH FDG-PET IMAGING TO PREDICT TREATMENT RESPONSE IN ADVANCED HODGKIN LYMPHOMA IN THE RATHL STUDY (CRUK/07/033). *Hematological Oncology* **35**, 91–92 (2017).

116. Scott, D. W. *et al.* THE 23-GENE GENE EXPRESSION-BASED ASSAY DOES NOT PREDICT INTERIM PET SCAN RESULTS AFTER ABVD IN ADVANCED STAGE CLASSICAL HODGKIN LYMPHOMA IN THE US INTERGROUP S0816 TRIAL. *Hematological Oncology* **35**, 92–93 (2017).

117. Calvente, L. *et al.* Validation of the RHL30 digital gene expression assay as a prognostic biomarker for relapsed Hodgkin lymphoma. *Br J Haematol* **190**, 864–868 (2020).

118. Peter Vandenberghe, Iwona Wlodarska, Thomas Tousseyn, Luc Dehaspe, Daan Dierickx, Magali Verheecke, Anne Uyttebroeck, Oliver Bechter, Michel Delforge, Vincent Vandecaveye, Nathalie Brison, Gregor E G Verhoef, Eric Legius, Frederic

Amant, Joris R Vermeesch. Non-invasive detection of genomic imbalances in Hodgkin/Reed-Sternberg cells in early and advanced stage Hodgkin's lymphoma by sequencing of circulating cell- free DNA: a technical proof-of-principle study. *Lancet Haematology* **2**, 55–65 (2015).

119. Spina, V. *et al.* Circulating tumor DNA reveals genetics, clonal evolution, and residual disease in classical Hodgkin lymphoma. *Blood* **131**, 2413–2425 (2018).

120. Sobesky, S. *et al.* In-depth cell-free DNA sequencing reveals genomic landscape of Hodgkin's lymphoma and facilitates ultrasensitive residual disease detection. *Med* **2**, 1171- 1193.e11 (2021).

121. Desch, A.-K. *et al.* Genotyping circulating tumor DNA of pediatric Hodgkin lymphoma. *Leukemia* **34**, 151–166 (2020).

122. Alig, S. K. *et al.* Distinct Hodgkin lymphoma subtypes defined by noninvasive genomic profiling. *Nature* **625**, 778–787 (2024).

123. Heger, J.-M. *et al.* Circulating Tumor DNA Sequencing for Biologic Classification and Individualized Risk Stratification in Patients With Hodgkin Lymphoma. *JCO* **42**, 4218– 4230 (2024).

124. NanoString Technologies. NanoString PanCancer Immune Profiling Panel. (2025).

125. Newman, A. M. *et al.* Robust enumeration of cell subsets from tissue expression profiles. *Nat Methods* **12**, 453–457 (2015).

126. Taki M, Abiko K, Ukita M, et al: Tumor Immune Microenvironment during Epithelial-Mesenchymal Transition. Clin Cancer Res 27:4669-4679, 2021

127. Wang G, Xu D, Zhang Z, et al: The pan-cancer landscape of crosstalk between epithelial-mesenchymal transition and immune evasion relevant to prognosis and immunotherapy response. NPJ Precis Oncol 5:56, 2021

128. Sanchez-Espiridion B, Montalban C, Lopez A, et al: A molecular risk score based on 4 functional pathways for advanced classical Hodgkin lymphoma. Blood 116:e12-7, 2010

129. Shanmugam V, Tokcan N, Chafamo D, et al: Genome-scale spatial mapping of the Hodgkin lymphoma microenvironment identifies tumor cell survival factors. bioRxiv, 2025

130. Aoki T, Jiang A, Xu A, et al: Spatially Resolved Tumor Microenvironment Predicts Treatment Outcomes in Relapsed/Refractory Hodgkin Lymphoma. J Clin Oncol 42:1077-1087, 2024